

To appear in *Ap.J.*

## An Unbiased Estimate of the Global Hubble Constant in the Region of Pisces-Perseus

Masaru Watanabe<sup>1</sup>

Department of Astronomy, University of Tokyo, Tokyo 113, Japan

Takashi Ichikawa<sup>2</sup>

Kiso Observatory, University of Tokyo, Nagano 397-01, Japan

and

Sadanori Okamura

Department of Astronomy, University of Tokyo, Tokyo 113, Japan

### ABSTRACT

We obtain an unbiased estimate of the global Hubble constant  $H_0$  in the volume of  $cz \leq 12000 \text{ km s}^{-1}$  in the region of Pisces-Perseus. The Tully-Fisher (TF) relation is applied to a magnitude-limited sample of 441 spirals selected from the Arecibo 21 cm catalog. We improve the photometry data of the previous TF study by Ichikawa and Fukugita (1992) by using our original surface photometry data and local calibrators which are newly made available in the literature. The photometry data were calibrated with CCD observations and we achieve 0.13 mag for a photometric internal error. We use a maximum likelihood method for the TF analysis. Monte-Carlo simulations demonstrate that our method reproduces a given  $H_0$  at the 95% confidence level. By applying the method to our sample galaxies, we obtain the unbiased global Hubble constant  $H_0 = 65 \pm 2^{+20}_{-14} \text{ km s}^{-1} \text{ Mpc}^{-1}$ ; the first and the second terms represent the internal random error and the external uppermost and lowermost systematic errors, respectively. We also find a good agreement for our  $H_0$  with those recently obtained via Cepheid observation in the local Universe and the TF relation and supernovae applied to a spatial volume comparable with or larger than ours. Hubble velocities of the spirals inferred from our  $H_0$  show no significant systematic difference from those given in the Mark III catalog. The same analysis for  $H_0$  is carried out using *r*-band photometry data of the Pisces-Perseus region given by Willick et al. (1997). We obtain a global  $H_0$  which is consistent with that obtained from the *B*-band analysis. A bulk motion in the Pisces-Perseus region is briefly discussed, based on our calibration of  $H_0$ . The *B*-band intrinsic TF scatter is too large to allow any determination of bulk motion. However, our *r*-band TF analysis supports the notion of a coherent streaming motion of the Pisces-Perseus ridge with  $\sim -200 \text{ km s}^{-1}$  with respect to the CMB, in agreement with most modern studies.

*Subject headings:* distance scale — galaxies: clusters : individual (Pisces-Perseus) — galaxies: distances and redshifts

---

<sup>1</sup>Present address : National Astronomical Observatory of Japan, Tokyo 181, Japan

<sup>2</sup>Present address : Astronomical Institute, Tohoku University, Sendai 980-77, Japan

## 1. Introduction

The global value of the Hubble constant  $H_0$  is determined by investigating a Hubble flow of a large number of galaxies distributed in a volume larger than the scale of inhomogeneous galaxy distribution in the Universe ( $\sim 100 h^{-1}$  Mpc,  $h \equiv H_0/100 \text{ km s}^{-1} \text{Mpc}^{-1}$ ). Ichikawa & Fukugita (1992, hereafter IF92) determined the global  $H_0$  by applying the Tully-Fisher (TF) relation (Tully & Fisher 1977) to the Arecibo HI 21 cm sample (Giovanelli and Haynes 1985, Giovanelli et al. 1986, Giovanelli and Haynes 1989). The sample extends in the area of 950 square-degrees in the region of Pisces-Perseus ( $22^h \leq \alpha_{1950} \leq 4^h$ ,  $+22^\circ \leq \delta_{1950} \leq +33^\circ$ ) and includes all the field and cluster galaxies complete down to  $m_z = 15.5$  mag originated from CGCG (Zwicky et al. 1961-68). Because of the large area and the deep limiting magnitude, the sample IF92 used contains about 400 spirals at  $cz \leq 12000 \text{ km s}^{-1}$ . This large sample enabled them to examine an effect of biases in the TF analysis.

In this paper, we re-determine  $H_0$  using the Arecibo HI sample. The differences from the study of IF92 are as follows. First, the imaging data were extracted from our photographic plate material via modern image reduction techniques. IF92 used magnitudes and axial ratios which were transformed into a homogeneous system of RC2 (de Vaucouleurs, de Vaucouleurs & Corwin 1976) from CGCG, UGC (Nilson 1973), and the Arecibo catalog. Second, we use a new set of local calibrators for TF calibration. Their distances are all calibrated with Cepheid observations. Third, our TF analysis uses a technique of maximum likelihood method. Fourth, our TF analysis is also applied to  $r$ -band CCD data of “w91pp” in the Mark III catalog (Willick et al. 1997). The sample was originated from UGC and hence complete down to  $m_z = 14.5$  mag, shallower than ours by 1 mag. Nevertheless, the data allow us to carry out a useful comparison with our result because the  $r$ -band TF relation is tighter than that of  $B$ -band. Finally, we discuss, based on our result of the global  $H_0$ , the bulk motion of galaxies in the region which has been studies by many authors (Willick 1990, Han and Mould 1992, Courteau et al. 1993, Hudson et al. 1997).

Our adoption of photographic data may deserve a comment. Motivation of the present study is to determine  $H_0$  in the Pisces-Perseus region where a bulk motion of galaxies has been attracted much attention (Willick 1991 ; Han and Mould 1992 ; Courteau et al. 1993 ; Hudson et al. 1997). The bulk motion has been usually computed using relative distances of galaxies with respect to a reference point of the Hubble flow. In this procedure, the motion is derived independently from  $H_0$ . In this paper, on the other hand, we attempt to determine the global  $H_0$  and then discuss the bulk flow using the absolute value of  $H_0$ .

To achieve the goal of our study, our galaxy sample should fulfill three conditions. First, it should be large in terms of the spatial volume so that the global  $H_0$  is determined unaffected by the bulk flow. The volume is required to be larger than the coherent scale of the flow ( $cz \sim 6000 \text{ km s}^{-1}$ ). Second, our sample should be also large in terms of the number of galaxies and should not be sparse so that we can evaluate the effect of a bias correctly. Third, it is of course highly desired that photometry data are homogeneous so as to eliminate systematic errors which creep in a data set taken from different compilations. Considering these conditions, we carried out photographic observations and obtained homogeneous photometry data for the Pisces-Perseus region. The galaxy sample is a magnitude limited one containing all the CGCG/UGC galaxies, and is distributed up to  $cz \sim 12000 \text{ km s}^{-1}$ . The sample is therefore larger than a Pisces-Perseus field sample “w91pp” in the Mark III catalog (Willick et al. 1997). A recent study of  $H_0$  by Giovanelli et al. (1997a) covered the entire sky using 24 clusters. Although the Pisces-Perseus region was included in their research, their sample in the region is limited to five clusters including about 150 galaxies. Further, the accuracy of our photographic photometry is as good as 0.13 mag (Watanabe

1996). It is worth stressing that careful photographic photometry do achieve 0.1-0.2 mag accuracy (e.g., Kodaira et al. 1990 ; Yasuda, Okamura and Fukugita 1995). Thus, our photographic observations offer the photometry data which are most suitable for our study.

Outline of this paper is as follows. The data used for the present analysis are described in §2. The maximum-likelihood method of the TF analysis is presented in §3. Calibration of the TF relation is given in §4. Reliability of the present method is examined by Monte-Carlo simulations in §5. The method is applied to our  $B$ -band sample and the unbiased estimate of the global  $H_0$  is determined in §6. A comparative analysis is carried out using “w91pp” data of Mark III compilation in §7. We discuss the present result in §8.

## 2. Data

### 2.1. Observations and Data Reduction

Observations and data reduction are briefly described here. Details will be given in a forthcoming paper.

Photographic observations of the region of Pisces-Perseus ( $22^h \leq \alpha_{1950} \leq 4^h$  and  $+22^\circ \leq \delta_{1950} \leq +33^\circ$ ) were carried out in  $B$  (Kodak IIa-O emulsion plus Schott GG385 glass filter) using the 105 cm Schmidt telescope at the Kiso Observatory, the University of Tokyo. Most of the observations were conducted in 1991 and in 1992 and we obtained thirty-eight plates. We measured and reduced all the 1524 CGCG and UGC galaxies in the region. These 1524 galaxies are referred to as the photometry sample. The galaxies were scanned with a PDS2020 microdensitometer at the Kiso Observatory. We then reduced the images in a conventional manner for Schmidt plate data (e.g., Kodaira et al. 1990) using the software packages IRAF<sup>3</sup> and SPIRAL (Ichikawa et al. 1987 ; Hamabe and Ichikawa 1991). CCD observations were also carried out in  $B$  and in  $V$  for seventy spirals selected from the photometry sample to calibrate the photographic data. The CCD data were calibrated with photometric standard stars (Landolt 1992) of various colors observed at various zenith distances to correct atmospheric extinction and to transform our photographic  $B$ -band system to the Johnson’s. For seven plates where no CCD observation was available, the flux calibration was made with photoelectric aperture photometry data of Longo and de Vaucouleurs (1983). The flux calibration of the photographic data using the CCD and the photoelectric aperture photometry data followed the conventional method of Kodaira et al. (1990). Aperture magnitudes were measured with a series of concentric circular apertures throughout the present study. Total magnitudes  $B_T$  were obtained by a sliding fit of aperture-magnitude curve (hereafter a growth curve) to their templates given in RC3 (de Vaucouleurs et al. 1991). Isophotal magnitudes  $B_{25}$  and major-to-minor axial ratios  $R_{25}$  were measured at the isophote of 25 mag arcsec $^{-2}$  in the surface brightness. Internal errors were 0.13 mag for  $B_T$  and 0.06 dex for  $\log R_{25}$  (Watanabe 1996).

Spiral galaxies are selected from the photometry sample and used for the present TF analysis. The procedure of the selection is described in §2.5.

---

<sup>3</sup>IRAF is distributed by the National Optical Astronomy Observatories, which is operated by the Association of Universities for Research in Astronomy, Inc. (AURA) under cooperative agreement with the National Science Foundation.

## 2.2. Comparisons with Other Data

We examine external consistency by comparing our data with those in RC3 (N=79) and Cornell et al. (1987) (N=8). All overlapping systems were rejected from the comparisons. We find possible errors in  $B_T$  of RC3 for PGC 5473 (CGCG 502-87, UGC 1045) and in  $B_T$  of RC3 and in  $B_{25}$  of Cornell et al. (1987) for PGC 3133 (Watanabe 1996). These galaxies are further rejected. The comparisons are presented in Fig.1 and Fig.2. From a regression analysis for RC3 data, we obtain  $B_T(\text{Kiso}) = B_T(\text{RC3}) + 0.02 \text{ mag}$  ( $\sigma = 0.16 \text{ mag}$ ) and  $\log R_{25}(\text{Kiso}) = \log R_{25}(\text{RC3}) + 0.00$  ( $\sigma = 0.07 \text{ dex}$ ). If we assume that the half of  $\sigma = 0.16 \text{ mag}$  is ascribed to the error in RC3, our  $B_T$  is supposed to be as accurate as 0.11 mag. This is compatible with our internal error of 0.13 mag for  $B_T$ . Rms errors of  $B_T$  between RC3 data and ours are 0.17 mag (N=46) for galaxies calibrated with our CCD observation while 0.14 mag (N=32) for those calibrated with the aperture photometry data by Longo and de Vaucouleurs (1983). The difference between these two values is insignificant, and we do not think the calibration by the aperture photometry data is poorer than that by the CCD data. A regression analysis for Cornell's data leads to  $B_{25}(\text{Kiso}) = B_{25}(\text{Cornell}) + 0.01 \text{ mag}$  ( $\sigma = 0.01 \text{ mag}$ ) and  $\log R_{25}(\text{Kiso}) = \log R_{25}(\text{Cornell}) - 0.01$  ( $\sigma = 0.04 \text{ dex}$ ). These good agreements with their CCD data demonstrate reliability of our photographic photometry data.

## 2.3. HI Data

HI 21 cm data are taken from the Arecibo HI catalog (Giovanelli and Haynes 1985, Giovanelli et al. 1986, Giovanelli and Haynes 1989), where line-profile widths are defined at the 50% level of the line mean intensity. The line widths  $W_{50}^{\text{obs}}$  and heliocentric recession velocities  $V_h$  both have an accuracy of about  $10 \text{ km s}^{-1}$ .

In earlier TF calibration, the 21 cm line-profile width has been defined with two schemes. One refers to the width  $W_{50}^{\text{obs}}$  as used in the Arecibo catalog, while the other adopted a width  $W_{20}^{\text{obs}}$  measured at the 20% level of the line peak intensity. We adopt the latter definition  $W_{20}^{\text{obs}}$  because most of the earlier TF calibrations have been made with this scheme (e.g., Aaronson et al. 1986, Bottinelli et al. 1987, Pierce and Tully 1988, Willick 1990, Pierce & Tully 1992, IF92). Adopting this schemes allows us to compare our TF calibration easily with those of the previous studies. We convert  $W_{50}^{\text{obs}}$  to  $W_{20}^{\text{obs}}$  using an empirical formula given by Willick (1991) ;

$$\log W_{20}^{\text{obs}} - 2.5 = 0.933 (\log W_{50}^{\text{obs}} - 2.5) + 0.019. \quad (1)$$

The relation has a dispersion of 0.02 dex. The uncertainty caused by this dispersion is less than 0.1 mag which is negligible compared with the intrinsic dispersion of the TF relation,  $\geq 0.3 \text{ mag}$ .

We determine the global  $H_0$  with reference to a rest frame of the cosmic microwave background (CMB) radiation. The heliocentric velocity  $V_h$  is accordingly transformed to  $V_c$  measured in the frame using CMB dipole anisotropy attributed to the solar motion of  $v = 365 \text{ km s}^{-1}$  toward  $(l, b) = (265^\circ, +48^\circ)$  relative to the CMB radiation field (Smoot et al. 1991). Let  $l_g$  and  $b_g$  be the galactic longitude and latitude of a particular galaxy. Then, the transformation is expressed as  $V_c = V_h + v_x + v_y + v_z$  where  $v_x = v \cos b \cos l \cos b_g \cos l_g$ ,  $v_y = v \cos b \sin l \cos b_g \sin l_g$ , and  $v_z = v \sin b \sin b_g$ , respectively.

The Arecibo catalog mainly refers to UGC for galaxy morphological types. For galaxies for

which the type was not available in UGC, authors of the Arecibo catalog determined the type from visual inspection of galaxy images on Palomar Schmidt plates or on Palomar Sky Survey prints. We take their morphological type with a notation  $T_{GH}$ .

## 2.4. Correction to the Observational Parameters

### 2.4.1. Apparent magnitudes

The observed magnitude  $B_T$  is corrected for Galactic and internal extinction and K-dimming. The Galactic extinction  $A_G$  is taken from a machine-readable extinction map made by David Burstein (hereafter referred to as BH). The internal extinction  $A_i$  and the K-dimming  $K$  are both evaluated following a prescription given in RC3. Corrected magnitude  $B_T^0$  is then given by  $B_T^0 = B_T - A_G - A_i - K$ .

There are various schemes used for evaluation of  $A_G$  (e.g., BH, RC2, RSA [Sandage and Tammann 1981]) and  $A_i$  (e.g., RC3, RC2, RSA, Bothun et al. [1985]). Systematic offset among these different schemes will be taken into account as a source of an error for  $H_0$  (§6.1).

### 2.4.2. Line-profile widths

The line-profile width  $W_{20}^{obs}$  is corrected for a projection and a cosmological broadening effects with

$$W_{20} = \frac{W_{20}^{obs}}{(1+z) \sin i}, \quad (2)$$

where inclination  $i$  of a spiral is estimated from  $R_{25}$  via a formula

$$\sin i = \left( \frac{1 - R_{25}^{-2}}{1 - R_0^{-2}} \right)^{\frac{1}{2}} \quad (3)$$

Dependence of the intrinsic major-to-minor axial ratio  $R_0$  on a galaxy type was investigated by some authors (e.g., Bottinelli et al. 1983, Fouqué et al. 1990, Giovanelli et al. 1997b). Some authors also favors a low value  $R_0 < 0.2$  (Giovanelli et al. 1994 ; Giovanelli et al. 1997b ; Willick et al. 1997). However, we use a conservative value  $R_0^{-1} = 0.2$  for all spirals following most of earlier analysis (Pierce and Tully 1988 ; Fukugita et al. 1991 ; Freudling, Martel and Haynes 1991 ; IF92 ; Han 1992 ; Pierce and Tully 1992 ; Bernstein et al. 1994 ; Bureau, Mould and Staveley-Smith 1996). We find that adopting a low value of  $R_0^{-1} = 0.13$  or introducing its type dependence results in an insignificant change in  $H_0$  by  $\sim 1 \text{ km s}^{-1} \text{Mpc}^{-1}$  in our analysis.

Giovanelli et al. (1997b) proposed a different formula for the correction of the line-profile width  $W_{50}$ . A similar formula could be worked out for  $W_{20}$ . However, we did not pursue this way. The ratio of their observed width  $W$  to the corrected width  $W_1$  is almost constant ; the mean of  $W/W_1$  is 1.07 with a scatter of only 0.07. It is reasonable to assume that the ratio would be nearly constant in case such a revision is made for  $W_{20}$ . Further, such a revision would change

$W_{20}$  of local calibrators as well as sample galaxies. Then, the effect of such a revision is likely to be canceled out.

## 2.5. Sample Selection

We select sample galaxies for our TF analysis according to selection criteria as follows; 1) Morphological type Sa-Sd, i.e.,  $3 \leq T_{GH} \leq 8$  and  $T_{GH} = 12$ . This criterion is adopted to exclude S0 and very late-type spirals unsuitable for the TF analysis. Galaxies classified to  $T_{GH} = 12$  are all regarded as Sb in the present analysis. 2) Inclination  $i \geq 45^\circ$ . For galaxies with  $i < 45^\circ$ , an uncertainty of the TF magnitude caused by an error of  $\Delta \log R_{25} = 0.06$  (Watanabe 1996) combined with a slope of 6.14 for our TF calibration (§4.1) exceeds 0.4 mag, which is no more negligible compared with the intrinsic dispersion of the TF relation. 3) Recession velocity  $V_c \geq 1000 \text{ km s}^{-1}$ . This criterion is adopted to avoid disturbance by a local peculiar velocity field with amplitude of several hundreds  $\text{km s}^{-1}$ . 4) Line-profile width  $2.30 \leq \log W_{20} < 2.75$ . As discussed in §4.1, the lower and the upper boundaries are originated from the range of  $\log W_{20}$  for the local calibrators we adopted.

These criteria reduced the photometry sample to 449 galaxies (Table 1). These are hereafter referred to as the spiral sample. The TF analysis is carried out using 441 galaxies among them (§6). The eight galaxies are discarded from the analysis because of their large deviation in the TF magnitude; this is discussed in §4.2. A wedge diagram for the spiral sample is shown in Fig.3, which illustrates that the sample covers a spatial volume up to  $V_c \simeq 12000 \text{ km s}^{-1}$ . Number distribution as a function of  $B_T$  is shown in Fig.4. The number ratio of the spiral sample to the photometry sample is almost constant over  $13 \leq B_T \leq 17 \text{ mag}$ . The spiral sample is therefore supposed to be a fair subset of the photometry sample.

## 3. A MAXIMUM LIKELIHOOD TECHNIQUE

If we obtain a TF distance  $r_{TF}$  using  $B_T^0$  and a TF magnitude  $M_{TF}$  as  $r_{TF} = 10^{(B_T^0 - M_{TF} + 5)/5} \text{ pc}$ , the most straightforward estimate of  $H_0$  may be a ratio  $V_c/r_{TF}$ . We hereafter call it as the Hubble ratio. For our spiral sample, however, a sample average of the Hubble ratios is not a correct estimate of the true global  $H_0$ . It is subject to a systematic error because the sample galaxies are biased toward intrinsically bright ones. This bias is originated from the facts that the intrinsic dispersion  $\sigma_{TF}$  of the TF relation is non-zero and that the spiral sample is a magnitude-limited sample. Consequently, a systematic error occurs in the sample average of the Hubble ratio. In this paper, we refer to this bias as a *sampling incompleteness* bias. We also take the *Malmquist* bias (Malmquist 1922) into account in the present analysis. The Malmquist bias is caused by a non-zero intrinsic dispersion of the TF relation combined with a conical shape of an observed volume for a unit solid angle. A detailed review for the two biases is found in Strauss and Willick (1995). Note that an error caused by the Malmquist bias is independent of a limiting magnitude, while an error caused by the sampling incompleteness bias depends basically on the limiting magnitude.

To determine a global  $H_0$  which is not affected by such systematic errors, we use a maximum likelihood method in the TF analysis. A similar technique was used by Han and Mould (1990) for an analysis of a Local Supercluster velocity field. The likelihood function is computed using a probability distribution of  $W_{20}$  rather than  $B_T$  since it is less affected by the sample incompleteness (e.g., Schechter 1980; Freudling et al. 1995, and references therein). This is equivalent to the

“inverse method” discussed by Strauss and Willick (1995).

### 3.1. Formulation

Let us consider a probability  $\mathcal{P}^{(i)}$  that the  $i$ -th spiral galaxy has a line-profile width  $W_{20}^{obs(i)}$  under the condition that it has a true absolute magnitude  $M_B^{(i)}$ , an inclination  $i^{(i)}$ , and a redshift  $z^{(i)}$ . Note that  $M_B^{(i)}$  is an unknown parameter. An intrinsic line-profile width  $W_{20}^{(i)}$  is obtained from  $W_{20}^{obs(i)}$ ,  $i^{(i)}$ , and  $z^{(i)}$  with equations (2) and (3). A TF magnitude  $M_{TF}^{(i)}$  corresponding to  $W_{20}^{(i)}$  is then obtained by the TF relation,

$$M_{TF}^{(i)} = A + B (\log W_{20}^{(i)} - 2.5). \quad (4)$$

On the other hand, the Hubble’s law gives an estimate for  $M_B^{(i)}$ , i.e.,

$$M_B^{(i)} = B_T^{0(i)} - 5 \log V_c^{(i)} + 5 \log h - 15 - \delta, \quad (5)$$

where  $V_c^{(i)}$  is given in unit of  $\text{km s}^{-1}$ . The additional term  $\delta$  is a correction for a systematic error caused by the Malmquist bias. If galaxies are uniformly distributed in space, the systematic error is  $\delta = (3 \ln 10/5) \sigma^2 = 1.38 \sigma^2$ , where  $\sigma$  is a random distance error expressed in term of a distance modulus. In the present analysis, the measure of the distance is  $V_c$  (equation (5)). Accordingly, the random distance error comes from a random error  $\Delta V_c$ , which is evaluated as a square root of a quadratic sum of a line-of-sight component of a random peculiar velocity of galaxies  $\sigma_{rand}$  and an observational error of the recession velocity  $\Delta V_h$ ,

$$\Delta V_c = \left[ \sigma_{rand}^2 + (\Delta V_h)^2 \right]^{\frac{1}{2}}. \quad (6)$$

Using  $\Delta V_c$ , we obtain  $\sigma = 5 \log e \cdot (\Delta V_c / V_c^{(i)})$ . The systematic error  $\delta$  caused by the *homogeneous* Malmquist bias is therefore given by

$$\delta = 15 \log e \cdot \left( \frac{\Delta V_c}{V_c^{(i)}} \right)^2. \quad (7)$$

An effect of a spatial *inhomogeneity* of galaxy distribution is discussed later in §5.2.

We assume that an intrinsic broadening of the TF relation follows a Gaussian function with a dispersion  $\sigma_{TF}$ . Then, using  $M_{TF}^{(i)}$  and  $M_B^{(i)}$ , we obtain the probability  $\mathcal{P}^{(i)}$  in a following form:

$$\mathcal{P}^{(i)} = \frac{1}{C^{(i)}} \exp \left[ -\frac{(M_{TF}^{(i)} - M_B^{(i)})^2}{2\sigma_{(i)}^2} \right], \quad (8)$$

where  $\sigma_{(i)}$  includes  $\sigma_{TF}$  and uncertainties of  $M_{TF}^{(i)}$  and of  $M_B^{(i)}$ , i.e.,

$$\sigma_{(i)} = \left[ \sigma_{TF}^2 + (\Delta M_{TF}^{(i)})^2 + (\Delta M_B^{(i)})^2 \right]^{\frac{1}{2}}. \quad (9)$$

The uncertainty  $\Delta M_{TF}^{(i)}$  is evaluated from equations (2), (3) and (4) as

$$\Delta M_{TF}^{(i)} = \left[ \left( \frac{\Delta W_{20}^{obs}}{W_{20}^{obs(i)}} \right)^2 + \left( \frac{\Delta V_h}{c + V_h^{(i)}} \right)^2 + \left( \frac{\ln 10 \cdot \Delta \log R_{25}}{R_{25}^{(i)2} - 1} \right)^2 \right]^{\frac{1}{2}}, \quad (10)$$

where  $c$  is the velocity of light. The uncertainty  $\Delta M_B^{(i)}$ , on the other hand, is computed from equation (5) as

$$\Delta M_B^{(i)} = \left[ (\Delta B_T^{0(i)})^2 + \left( 5 \log e \cdot \frac{\Delta V_c}{V_c^{(i)}} \right)^2 \right]^{\frac{1}{2}}. \quad (11)$$

With the selection criterion  $2.30 \leq \log W_{20} < 2.75$  (§2.5), the factor  $C^{(i)}$  is computed by

$$C^{(i)} = \int_{M_{TF}^l}^{M_{TF}^u} \exp \left[ -\frac{(x - M_B^{(i)})^2}{2\sigma_{(i)}^2} \right] dx, \quad (12)$$

where  $M_{TF}^l$  and  $M_{TF}^u$  are TF magnitudes corresponding to the boundaries of  $\log W_{20} = 2.30$  and  $2.75$ , respectively.

The logarithmic likelihood function is finally obtained as

$$\begin{aligned} \log \mathcal{L} &= \log \prod_i \mathcal{P}^{(i)} \\ &= -\log e \cdot \sum_i \frac{(M_{TF}^{(i)} - M_B^{(i)})^2}{2\sigma_{(i)}^2} - \sum_i \log C^{(i)}. \end{aligned} \quad (13)$$

The most probable values for parameters in question are determined by maximizing  $\log \mathcal{L}$ .

We first apply the method to local calibrators to calibrate the TF relation (§4.1). In this case, we let  $A$ ,  $B$  in equation (4) and  $\sigma_{TF}$  in equation (9) be free parameters. The method is then applied to our TF sample (§6) with the calibrated TF relation to determine the unbiased  $H_0$ . In this case, we let  $h$  in equation (5) and  $\sigma_{TF}$  in equation (9) be free parameters.

There are five preset parameters to specify in our method;  $\Delta W_{20}^{obs}$ ,  $\sigma_{rand}$ ,  $\Delta V_h$ ,  $\Delta \log R_{25}$ , and  $\Delta B_T^0$ . When the method is applied to local calibrators, values for  $\Delta W_{20}^{obs}$ ,  $\Delta \log R_{25}$ , and  $\Delta B_T^0$  are taken from RC3. The parameters  $\sigma_{rand}$  and  $\Delta V_h$  are unnecessary in this case because we do not use equation (5) but use a known distance modulus to obtain  $M_B$  for local calibrators. When the method is applied to our TF sample, on the other hand, following values are used in common to all the galaxies in the sample.  $\Delta W_{20}^{obs} = 20 \text{ km s}^{-1}$ , which is estimated as a square root of a quadratic sum of a measurement error  $\sim 10 \text{ km s}^{-1}$  for  $W_{50}^{obs}$  (Giovanelli and Haynes 1985) and an uncertainty  $\sim 15 \text{ km s}^{-1}$  associated with the line-profile width conversion by equation (1).  $\sigma_{rand} = 300 \text{ km s}^{-1}$ , which is taken from Davis and Peebles (1983), de Lapparent, Geller and Huchra (1988) and Fisher et al. (1994).  $\Delta V_h = 10 \text{ km s}^{-1}$  is taken from Giovanelli and Haynes (1985).  $\Delta \log R_{25} = 0.06$  is taken from our error assessment (Watanabe 1996).  $\Delta B_T^0 = 0.16 \text{ mag}$ , which is evaluated as a square root of a quadratic sum of our photometric uncertainty  $\Delta B_T = 0.13 \text{ mag}$  (Watanabe

1996) and uncertainties  $\Delta A_G = 0.07$  mag and  $\Delta A_i = 0.05$  mag which is evaluated from  $\Delta \log R_{25}$ . Uncertainties of these values for the five preset parameters are taken into account in an assessment of an external error for  $H_0$  (§6.1).

## 4. THE TULLY-FISHER RELATION

### 4.1. Calibration

The TF relation is calibrated using local calibrators whose distances have been determined with Cepheid variables. These calibrators are further restricted to those which meet the same selection criteria as imposed on the Pisces-Perseus galaxies, i.e., a morphological type Sa-Sd and an inclination  $i \geq 45^\circ$  (§2.5). Ten spirals meet the criteria and are listed in Table 2. Among the ten calibrators, NGC 224, 598, and 3031 were recently suspected to be unsuitable for the TF calibration because of perturbations in the internal velocity field (Giovanelli et al. 1997a). Further we find that NGC 1365 and 4639 show large difference in their inclination between RC3 and Giovanelli et al. (1997a) ( $i = 59^\circ$  and  $48^\circ$  for NGC 1365 and  $i = 49^\circ$  and  $55^\circ$  for NGC 4639). We therefore exclude the five galaxies and use the remaining five as a fiducial set of calibrators. Calibration using all the ten calibrators gives only slight change in the following analysis. The alternative result is mentioned when necessary.

Distance moduli  $\mu^{(i)}$  of the calibrators are taken from the literature (Table 2). These distances are all based on the LMC distance modulus of 18.5 mag (e.g., Madore and Freedman 1991). Other observational data are all taken from RC3. Using  $\mu^{(i)}$  and apparent magnitudes  $B_T^{0(i)}$ , absolute magnitudes  $M_B^{(i)}$  of the local calibrators are given by

$$M_B^{(i)} = B_T^{0(i)} - \mu^{(i)}. \quad (14)$$

A TF diagram of the calibrators is shown in Fig.5. The range of  $W_{20}$  covered by the local calibrators,  $2.30 \leq \log W_{20} \leq 2.75$ , is already adopted as one of the selection criteria for the spiral sample (§2.5). Letting A, B and  $\sigma_{TF}$  be free parameters, we apply the maximum likelihood method and then obtained the following calibration ;

$$M_{TF}^{(B)} = -19.73 (\pm 0.20) - 6.14 (\pm 1.60) (\log W_{20} - 2.5). \quad (15)$$

The scatter  $\sigma_{TF}$  is 0.45 mag. If we use all the ten calibrators, we obtain  $A = -19.67 \pm 0.15$ ,  $B = -5.78 \pm 0.95$ , and  $\sigma_{TF} = 0.44$  mag. Our slopes are both consistent with that obtained by Strauss & Willick (1995) ( $B = -5.3$ ) within the errors, while the values are marginally smaller than that given by Pierce & Tully (1992) ( $B = -7.48$ ). This discrepancy is ascribed to the lack of our calibrators with  $\log W_{20} < 2.30$  that were used by them.

### 4.2. Examination of the TF Magnitude of the Spiral Sample

In determination of  $M_{TF}^{(B)}$ , the inclination  $i$  is the only observable derived from our measurements (equation [3]). To examine an error in  $M_{TF}^{(B)}$  caused by an error of our  $R_{25}$ , we plot in Fig.6 the residual  $M_{TF}^{(B)} - M_B$  as a function of  $\log R_{25}$ . The absolute magnitude  $M_B$  is

computed from the Hubble’s law (equation (5)) with  $H_0$  arbitrarily assumed to be  $\log h = -0.15$  ( $H_0 = 70.8 \text{ km s}^{-1}\text{Mpc}^{-1}$ ). Accordingly, a global offset of the plot from a horizontal line of  $M_{TF}^{(B)} - M_B = 0$  is of little significance. We found no significant systematic trend for  $M_{TF}^{(B)} - M_B$  as a function of  $\log R_{25}$  but found several deviant galaxies. Dispersion of the plot is 0.53 mag and, if we assume a Gaussian distribution for  $M_{TF}^{(B)} - M_B$  for 449 galaxies, less than 0.5 galaxies fall in the range out of  $3.06\sigma$ . Accordingly, deviation larger than  $|M_{TF}^{(B)} - M_B| = 1.62$  mag is considered to be significant, and we find eight galaxies out of the boundaries. Four out of the eight have possible reasons for the deviation as follows. PGC 6802 has very low surface brightness and then unreliable  $B_T$  and  $R_{25}$ . PGC 10013 has a very wavy growth curve which led unreliable  $B_T$ . PGC 10740 is extremely faint ( $B_T = 17.09$  mag) and hence its photometry may be unreliable. PGC 14033 suffers from severe contamination of HI flux of nearby galaxies (Giovanelli and Haynes 1985). We discard these from the TF analysis. Although we found no reason for the large deviation to the remaining four galaxies, we further exclude them from the TF analysis and hereafter refer to the remaining 441 galaxies as the TF sample (Table 1). An effect of including the latter four galaxies is mentioned when necessary. The velocity-distance relation is shown in Fig.7, where global agreement with the Hubble’s law is evident.

## 5. MONTE-CARLO SIMULATIONS

### 5.1. Simulated Sample

Evaluation of the effect of biases is an important issue in this study. However, it is quite difficult to evaluate the effect analytically because physical properties, spatial distribution, and observational limits for galaxies are entangled so complicatedly. For this purpose, a Monte-Carlo simulation provides a straightforward and convincing test (e.g., Kolatt et al. 1996).

We perform Monte-Carlo simulations using pseudo samples of 441 galaxies. These samples are made with unknown parameters given a priori as  $\log h = -0.15$  ( $H_0 = 70.8 \text{ km s}^{-1}\text{Mpc}^{-1}$ ) and  $\sigma_{TF} = 0.40$  mag. Procedure of assigning observational parameters to individual galaxies is described below.

Galaxies are distributed uniformly with respect to a pure Hubble flow velocity  $V_H$ . In the range of  $4000 \leq V_H < 5000 \text{ km s}^{-1}$ , five times as many galaxies as those in the uniform background are added to imitate the clustering feature of the Pisces-Perseus supercluster. Galaxies in  $1000 \leq V_H < 4000 \text{ km s}^{-1}$  are randomly discarded so that the number density becomes one third of that of the uniform background so as to model the low number density space in the foreground of the supercluster (Haynes and Giovanelli 1986). A true distance is given to the galaxies via the Hubble’s law with  $V_H$  and  $\log h = -0.15$ . We then define a velocity  $V_c$  by adding to  $V_H$  a Gaussian random motion with dispersion of  $\sigma_{rand} = 300 \text{ km s}^{-1}$  (Davis and Peebles 1983, de Lapparent, Geller and Huchra 1988, Fisher et al. 1994). Note that observers know neither  $V_H$  nor the true distance, but only  $V_c$  by observations as described later in this section.

Absolute magnitudes are assigned to the galaxies according to a galaxian luminosity function. Since our maximum likelihood analysis is little affected by the luminosity function, it is unnecessary to pursue its true (unknown) shape and amplitude. We adopted a Schechter form with  $M_B^* = -20.0$  mag and  $\alpha = -1.1$ , which are representative values found in recent studies (Efstathiou, Ellis and Peterson 1988; Loveday et al. 1992; Marzke, Huchra and Geller 1994). Then, an intrinsic HI line-profile width  $W$  is computed from the absolute magnitude and the

TF relation given by equation (15). It is assumed that the TF relation is broadened by its own intrinsic scatter with a Gaussian probability function of  $\sigma_{TF} = 0.40$  mag. Inclination  $i$  is assigned so that the galaxies have random orientation. Using  $W$ ,  $i$ , and  $V_c$ , a projected line-profile width  $W^{obs}$  is obtained via equation (2). Given the intrinsic axial ratio  $R_0^{-1} = 0.2$ , an axial ratio  $R$  is derived from the inclination using equation (3). An apparent magnitude  $B_T^0$  is derived from the absolute magnitude and the true distance. Internal extinction and K-dimming are computed according to a prescription given in RC3.

Now, these simulated galaxies are *observed*. The virtual observation imposes observational errors to the parameters and to reduce the sample according to a limiting magnitude. First, observational errors are added to  $V_c$ ,  $W^{obs}$ ,  $R$ , and  $B_T^0$ . The errors are assumed to follow random Gaussians whose dispersions are estimated from the actual TF sample galaxies. Following values are used for the dispersions :  $\Delta V = 10 \text{ km s}^{-1}$ ,  $\Delta W^{obs} = 20 \text{ km s}^{-1}$ ,  $\Delta \log R = 0.06$ , and  $\Delta B_T^0 = 0.16$  mag (§3.1). The simulated galaxies are then selected according to a limiting magnitude. A selection function  $\mathcal{S}(B_T)$  is defined as

$$\mathcal{S}(B_T) = \begin{cases} 1 & (B_T < 15.0 \text{ mag}) \\ N(B_T)/N_0 10^{0.6 B_T} & (15.0 \leq B_T < 17.0 \text{ mag}) \\ 0 & (B_T \geq 17.0 \text{ mag}), \end{cases} \quad (16)$$

where  $N(B_T)$  is the number of galaxies in the actual TF sample as a function of  $B_T$  (Fig.4). The normalization factor  $N_0$  is determined by a least-squares fit of  $N = N_0 \cdot 10^{0.6 B_T}$  to the number distribution of the subsample of  $B_T < 15.0$  mag shown in Fig.4.

Finally, according to the same selection criteria as imposed on the actual TF sample, i.e.,  $V_c \geq 1000 \text{ km s}^{-1}$ ,  $i \geq 45^\circ$  and  $2.30 \leq \log W_{20} < 2.75$ , the simulated magnitude-limited sample is reduced to generate a simulated TF sample of 441 galaxies. A velocity-TF distance relation of a typical example of the simulated TF samples is shown in Fig.8.

## 5.2. Examination of the Performance of the Present Method

Our TF analysis with the maximum likelihood method is applied to one hundred different simulated TF samples. We show in Fig.9 a probability contour map for  $H_0$  and  $\sigma_{TF}$  obtained for one of the simulated samples. The contours represent only an internal error associated with the likelihood calculation. The input values  $\log h = -0.15$  and  $\sigma_{TF} = 0.40$  mag are reproduced within the internal error of the maximum likelihood method (70% confidence level). A distribution of the most probable values of  $(H_0, \sigma_{TF})$  is shown in Fig.10 for the one hundred simulated samples. Also shown is a distribution of sample averages of  $\log(V_c/r_{TF})$  for the same samples. In this case, the intrinsic scatter  $\sigma_{TF}$  is tentatively taken equal to the value obtained by the maximum likelihood method. It is clearly demonstrated that the sample average of  $\log(V_c/r_{TF})$  is subject to a significant systematic error. The  $H_0$ 's derived from the maximum likelihood method, on the other hand, show a distribution consistent with the input value.

We further examine the performance of our method by computing a spatial variation of  $H_0$  with a simulated TF sample divided into bins of  $\log V_c$ . The intrinsic scatter  $\sigma_{TF}$  is fixed for all the subsamples in the  $\log V_c$  bins at 0.41 mag obtained from the analysis shown in Fig.9. The variation of  $H_0$  is shown in Fig.11a. The evident increase of the sample average of  $\log(V_c/r_{TF})$  with  $\log V_c$  demonstrates the effect of the sampling incompleteness bias. The apparent increase manifests

itself as the systematic error shown in Fig.10. It is evident, on the other hand, that the maximum likelihood method is free from the systematic error caused by the sampling incompleteness bias and gives unbiased estimates of  $H_0$ 's regardless of  $\log V_c$ .

As shown in equation (5), we corrected for the Malmquist bias assuming an uniform galaxy distribution although the actual distribution is inhomogeneous. To examine the effect of ignoring the inhomogeneity, we made a comparative simulation using a uniform galaxy distribution. A resultant variation of  $H_0$  is shown in Fig.11b. Comparison of the two results would reveal the effect of inhomogeneity, if any, as a residual. However, we observe no significant difference between the two results. Accordingly, we neglect the correction for the inhomogeneous Malmquist bias in the present analysis.

## 6. RESULT

### 6.1. Global Value of $H_0$

The maximum likelihood method is applied to our TF sample. The resultant probability contour map for  $H_0$  and  $\sigma_{TF}^{(B)}$  is shown in Fig.12. Note that the contours represents only the internal error of the likelihood calculation. Other error sources are as follows. A zero point uncertainty of the TF calibration is evaluated from the standard deviation of the calibrators around the TF relation, i.e.,  $0.45/\sqrt{5} = 0.20$  mag (§4.1). The systematic difference of  $A_G$  is examined among the schemes of BH, RC2, and RSA (Sandage and Tammann 1981), and the difference of  $A_i$  is examined among RC3, RC2, RSA and Bothun et al. (1985). The result is summarized in Table 3. Since the same absorption correction schemes are used both for the TF sample and for the local calibrators, scheme dependence tends to cancel out. The maximum differences in  $A_G$  and in  $A_i$  are adopted as the respective external errors. These external systematic errors are summarized in Table 4.

Finally, we obtain the best estimate of the unbiased global  $H_0$  as

$$H_0 = 65 \pm 2^{+20}_{-14} \text{ km s}^{-1} \text{Mpc}^{-1}. \quad (17)$$

The first and the second terms of the quoted errors represent the internal random error of the maximum likelihood method and the external systematic error, respectively. Note that the latter is given by the uppermost and the lowermost boundaries of the *linear* sum. The errors of  $H_0$  are often underestimated by ignoring various complicated systematic effects. Our error estimate is the result of our best effort to include all the known error sources with conservative error budgets assigned to respective sources. The intrinsic scatter of the *B*-band TF relation is obtained to be  $\sigma_{TF}^{(B)} = 0.49 \pm 0.05$  mag. An analysis with the ten calibrators results in  $H_0 = 68 \text{ km s}^{-1} \text{Mpc}^{-1}$  with  $\sigma_{TF}^{(B)} = 0.48$  mag. If we use 445 galaxies including four spirals discarded from the TF sample (§4.2),  $\sigma_{TF}^{(B)}$  slightly increases to 0.54 mag but  $H_0$  does not change in practice.

### 6.2. Spatial Variation of $H_0$

A spatial variation of  $H_0$  is examined using the TF sample divided into bins of  $\log V_c$ . Dispersion  $\sigma_{TF}^{(B)}$  is fixed at 0.49 mag for all the subsamples in the bins; the free parameter is only  $H_0$  in the maximum likelihood method here. The spatial variation obtained is shown in Fig.13.

It is clearly demonstrated that the sample means of  $\log(V_c/r_{TF}^{(B)})$  are seriously subject to the systematic error as  $V_c$  increases. On the other hand, the amplitude of the variation of  $H_0$ 's is consistent with the global  $H_0$  within the errors except for poor subsamples at  $\log V_c < 3.6$ .

## 7. ANALYSIS WITH WILLICK'S r-BAND DATA

### 7.1. r-band Sample

The same  $H_0$  determination is carried out using  $r$ -band CCD data of the Pisces-Perseus region given by Willick et al. (1997). The sample (w91pp) is based on UGC and consists of 326 spirals complete down to  $m_z = 14.5$  mag. Application of the same selection criteria as used in our TF analysis to w91pp reduced the sample to 271 galaxies. We hereafter refer to this sample of 271 galaxies as the  $r$ -band TF sample. The velocity distribution is shown in Fig.14. The shallower limiting magnitude than ours ( $m_z = 15.5$  mag) makes the spatial coverage of this sample less extensive than that of the  $B$ -band sample (Fig.3).

### 7.2. r-band TF calibration

The  $r$ -band TF relation was calibrated with six local calibrators (Table 2). The same criteria as in  $B$ -band leave only two local calibrators (NGC 1365 and 2403). We do not exclude NGC 224, 300, 598 and 3031 simply because the two calibrators are insufficient for reasonable calibration. Photometry data for NGC 1365 are taken from ESO-Uppsala catalog (Lauberts and Valentijn 1989) while the data for the others are from Pierce and Tully (1992). Kron-Cousins  $R$  and  $I$  magnitudes are transformed with a color equation  $r = 0.40 + R - 0.28(R - I)$  given by Willick (1991). Total magnitudes  $r_T$  were corrected for  $A_G$  and  $A_i$  using BH and Bothun et al. (1985), respectively, with a transformation  $A^{(r)} = 0.60A^{(B)}$ . Corrected apparent magnitudes  $r_T^0$  are given in Table 2. With the maximum likelihood method, the  $r$ -band TF relation is obtained as

$$M_{TF}^{(r)} = -20.15 (\pm 0.18) - 7.93 (\pm 1.04) (\log W_{20} - 2.5). \quad (18)$$

The TF diagram of the local calibrators is shown in Fig.15. The dispersion is 0.42 mag. The slope is consistent with that of Pierce & Tully (1992), although we found inconsistency in  $B$  (§4.1). This is because the  $r$ -band TF diagram in Pierce & Tully (1992) shows no appreciable difference in slope between  $\log W_{20} > 2.30$  and  $\log W_{20} < 2.30$ , which is not the case in the  $B$ -band. Willick et al. (1997) gave 7.73 for the slope, which also matches well with ours. Our correction for  $A_i$  and for  $A_G$  follows the same schemes as theirs, thus the zero point of the TF calibration is also comparable with ours. Their zero point is  $-20.12$  ( $H_0 = 65 \text{ km s}^{-1} \text{Mpc}^{-1}$  assumed), which is in good agreement with ours.

A systematic difference of  $\Delta \log R_{25} = 0.03$  is found between our axial ratio  $R_{25}$  and that measured by Willick (1991) (Fig.16). This difference introduces errors of 0.03-0.45 mag in  $A_i$  and 0.3-7 % in  $W_{20}$  depending on galaxy morphology and inclination, respectively. A comparative calculation using both sets of the axial ratios for galaxies common between the  $r$ - and the  $B$ -band samples shows that our axial ratios gives  $H_0$  which is 3% smaller than that in  $r$ .

The velocity-distance relation for the  $r$ -band TF sample is shown in Fig.17. We find that the  $r$ -band sample shows tighter velocity-distance correlation (correlation coefficient = 0.873)

than for  $\mu_{TF}^{(B)}$  (correlation coefficient = 0.804, Fig.7). This may be accounted for by the following two reasons. First, the  $r$ -band TF relation shows smaller intrinsic scatter than  $B$ -band (Pierce and Tully 1988). Second, the CCD observations for the  $r$ -band sample provide more accurate photometry than our photographic photometry.

Difference between  $\mu_{TF}^{(r)}$  and  $\mu_{TF}^{(B)}$  is plotted against  $\log V_c$  in Fig.18. There is a systematic difference of 0.16 mag. If this is ascribed to the Malmquist bias, i.e.,  $1.38(\sigma_{TF}^{(B)2} - \sigma_{TF}^{(r)2}) = 0.16$  mag, then we obtain  $\sigma_{TF}^{(r)} = 0.35$  mag from  $\sigma_{TF}^{(B)} = 0.49$  mag (§6.1), This value is indeed in agreement with what we obtain in the following maximum likelihood analysis (§7.3).

Note that the  $r$ -band calibrators miss NGC 925 and 4536 which show relatively large deviation in  $B$  from the calibrated relation (Table 2). It is possible that future inclusion of these galaxies considerably changes our  $r$ -band result.

### 7.3. Result

A contour map for  $H_0$  and  $\sigma_{TF}^{(r)}$  obtained from the maximum likelihood analysis is shown in Fig.19. The internal and external errors are assessed in the same way as for the  $B$ -band sample. We finally obtain

$$H_0 = 63 \pm 1 \pm 13 \text{ km s}^{-1} \text{Mpc}^{-1}. \quad (19)$$

The quoted errors have the same meaning as equation (17). The intrinsic scatter of the  $r$ -band TF relation is obtained to be  $\sigma_{TF}^{(r)} = 0.33 \pm 0.05$  mag. This  $\sigma_{TF}^{(r)}$  well explains the systematic difference between  $\mu_{TF}^{(r)}$  and  $\mu_{TF}^{(B)}$  shown in Fig.18.

The spatial variation of  $H_0$  is shown in Fig.20. Except for poor subsamples at  $\log V_c < 3.5$ , the values of  $H_0$ 's are mostly in agreement with the global value within their errors. Apparent increase of a sample mean of  $\log(V_c/r_{TF}^{(r)})$  toward larger  $\log V_c$  is smaller than that for  $B$ -band analysis (Fig.13). This is consistent with  $\sigma_{TF}^{(r)}$  which is smaller than  $\sigma_{TF}^{(B)}$ .

## 8. DISCUSSION

### 8.1. Global Value of $H_0$

We compare our result with those obtained by other studies from the TF relation, the period-luminosity relation of Cepheid variables, surface brightness fluctuation (SBF), the planetary nebulae luminosity function (PNLF), and supernovae (SNe) type Ia and II. Extensive reviews for these methods are found in Jacoby et al. (1992), van den Bergh (1994), Livio, Donahue and Panagia (1997), and Okamura (1998).

#### 8.1.1. The Tully-Fisher relation

IF92 obtained  $H_0 = 78.5 \pm 10.3 \text{ km s}^{-1} \text{Mpc}^{-1}$  using the TF relation calibrated with five calibrators (NGC 224, 598, 300, 2403, 3031). If we adopt the same calibrators as theirs but new Cepheid distances, we obtain a TF calibration of  $M_{TF}^{(B)} = -19.44 - 6.19(\log W_{20} - 2.5)$ . The slope

matchs that of IF92,  $-6.24$ , but the zero point is  $0.28$  mag brighter. Using this calibration, we obtain  $H_0 = 74 \pm 2^{+17}_{-10} \text{ km s}^{-1} \text{Mpc}^{-1}$ . The difference of  $H_0$  between IF92 and this calculation is fully ascribed to the TF zero point difference of  $0.28$  mag.

The Mark III catalog (Willick et al. 1997) provides Hubble velocities of spirals using the TF relation. For our galaxies common to the Mark III “w91pp” and “hmcl” samples, we compute the Hubble velocities using  $H_0^{(B)} = 65 \text{ km s}^{-1} \text{Mpc}^{-1}$  and our TF distance moduli  $r_{TF}^{c(B)}$  corrected for the Malmquist bias. The result of comparison is shown in Fig.21. No systematic difference is found in the Hubble velocity, except for a bin  $3.5 \leq \log V_{MB} < 3.6$  of w91pp. For this bin, we observe  $H_0$  which is larger than those of other bins (Fig.13). This locally larger value of  $H_0$  is compatible with the difference of the Hubble velocity in this bin. These facts imply an actual infall motion of galaxies in the bin toward the Pisces-Perseus supercluster.

Recently, Giovanelli et al. (1997a) studied 24 clusters of galaxies out to  $V_c \sim 9000 \text{ km s}^{-1}$  and obtained  $H_0 = 69 \pm 5 \text{ km s}^{-1} \text{Mpc}^{-1}$ . Our result  $H_0^{(B)} = 65 \text{ km s}^{-1} \text{Mpc}^{-1}$  is in good agreement with theirs. Four of their clusters reside in the Pisces-Perseus region we observed. A comparison of the galaxy distances is shown in Fig.22. Their distance modulus here is converted from their original recession velocity (Giovanelli et al. 1997b) based on  $H_0 = 69 \text{ km s}^{-1} \text{Mpc}^{-1}$ . The systematic difference is  $-0.06$  mag, indicating a satisfactory agreement in the distances. A vertical spread is apparent at  $m - M = 34.4$ . The spread,  $\Delta(m - M) \sim 0.5$  mag, is consistent with our TF dispersion  $\sigma_{TF}^{(B)} = 0.49 \pm 0.05$  mag.

### 8.1.2. Other Methods

The period-luminosity relation of Cepheid variables, SBF, and PNLF are currently available to galaxies up to only a few tens of Mpc. Using Cepheids in galaxies in the Virgo cluster, Pierce et al. (1994) and Freedman et al. (1994) obtained  $H_0 = 87 \pm 7$  and  $80 \pm 17 \text{ km s}^{-1} \text{Mpc}^{-1}$ , respectively. The error quoted by Pierce et al. (1994) did not include the cluster depth effect for which Freedman et al. (1994) assumed  $\pm 0.35$  mag. If the same depth effect is taken into account in the result of Pierce et al. (1994), the total error becomes  $\pm 17 \text{ km s}^{-1} \text{Mpc}^{-1}$ . Tanvir et al. (1995) identified Cepheid variables in a galaxy in the Leo I group and obtained a smaller value  $H_0 = 69 \pm 8 \text{ km s}^{-1} \text{Mpc}^{-1}$ . More recently, Freedman (1998) presented  $H_0 = 73 \pm 14 \text{ km s}^{-1} \text{Mpc}^{-1}$  in an interim report of the HST key project. From the SBF method with a new zero point calibrated with Cepheid observations, Tonry et al. (1997) obtained  $H_0 = 81 \pm 6 \text{ km s}^{-1} \text{Mpc}^{-1}$ . Using the PNLF method, McMillan, Ciardullo and Jacoby (1993) obtained from three galaxies in the Fornax cluster  $H_0 = 81 \pm 8 \text{ km s}^{-1} \text{Mpc}^{-1}$  and  $69 \pm 8 \text{ km s}^{-1} \text{Mpc}^{-1}$ , which depend on the choice of the Fornax/Coma distance ratio of 5.25 (Faber et al. 1989) and 6.14 (Aaronson et al. 1989), respectively. Although PNLF distances are based on the M31 distance of 710 kpc instead of 770 kpc which we adopt, the difference reduces their  $H_0$ ’s by only 3%.

Using a Hubble diagram of 13 SNe type Ia calibrated with a single Cepheid distance to SN 1972E in NGC 5253, Riess, Press and Kirshner (1995) obtained  $H_0 = 67 \pm 7 \text{ km s}^{-1} \text{Mpc}^{-1}$  within  $V_c \sim 30000 \text{ km s}^{-1}$ . Hamuy et al. (1996) obtained  $H_0 = 63.1 \pm 3.4 \pm 2.9 \text{ km s}^{-1} \text{Mpc}^{-1}$  in a similar spatial extent using a Hubble diagram constructed with 29 SNe of type Ia and calibrated with four SNe (SN 1972E in NGC 5253, SN 1937C in IC 4182, and SN 1981B in NGC 4536, and SN 1990N in NGC 4639) to which Cepheid distances are available. These  $H_0$ ’s are both in good agreement with ours (see also Saha et al. 1995, Tammann and Sandage 1995, Saha et al. 1996). The expanding photosphere method has been developed for the distance determination with type

II SNe (Kirshner and Kwan 1974). The method directly provides the distance to the SNe without any external calibration procedures. Schmidt et al. (1994) obtained  $H_0 = 73 \pm 6 \pm 7 \text{ km s}^{-1} \text{Mpc}^{-1}$  using sixteen SNe type II extending to  $V_c \sim 15000 \text{ km s}^{-1}$ . Their result is slightly larger than but in marginal agreement with ours.

Shanks (1997) compared TF distances to 11 spirals with their Cepheid distances and to 12 spirals with their SNe Ia distances. The TF distances were taken from Pierce (1994). They concluded that, overall, the TF distance is smaller by  $0.43 \pm 0.11$  mag than the Cepheid/SNe distances. This leads to that  $H_0$  obtained by Pierce (1991) using the Virgo and the Ursa Major clusters is revised downwards from  $H_0 = 84 \pm 10 \text{ km s}^{-1} \text{Mpc}^{-1}$  to  $H_0 = 69 \pm 8 \text{ km s}^{-1} \text{Mpc}^{-1}$ . This  $H_0$  is in good agreement with ours.

From the above overview, our  $H_0 = 65 \pm 2^{+20}_{-14} \text{ km s}^{-1} \text{Mpc}^{-1}$  agrees with the results by Cepheids observations, the SNe Ia and II and the Tully-Fisher relation. Although sample galaxies are sparse, Cepheids and SNe observations currently provide us with the most reliable distances in the local Universe ( $\sim 20 h^{-1} \text{ Mpc}$ ) and to much further galaxies ( $\sim 500 h^{-1} \text{ Mpc}$ ), respectively. It is a good demonstration that our estimate of the global  $H_0$  is consistent with both of these results obtained from such different fields of the Universe. It is also convincing that our  $H_0$  is in agreement with the result of an independent TF study, Giovanelli et al. (1997a), which used sparse but widely distributed galaxies. Further comparative studies of the Cepheid, SBF, and PNLF distances will work out the current inconsistency of  $H_0$  among these three methods. Then, Cepheid observations of distant galaxies will give a definite conclusion for the global value of  $H_0$ .

## 8.2. Bulk Motion

A bulk motion in the Pisces-Perseus region was investigated by Willick (1990), Han and Mould (1992), Courteau et al. (1993), Baffa et al. (1993), and Hudson et al. (1997). Willick (1990) claimed that the Pisces-Perseus supercluster and the galaxies behind the supercluster up to  $V_c \sim 8000 \text{ km s}^{-1}$  showed a negative coherent flow. The result was supported by Courteau et al. (1993), who argued that all galaxies within a sphere out to at least  $V_c \sim 6000 \text{ km s}^{-1}$  in radius around the Local Group showed parallel streaming flow with amplitude of  $\sim -400 \text{ km s}^{-1}$  toward the Great Attractor. Han and Mould (1992) studied clusters of galaxies lying beyond the Pisces-Perseus supercluster, and also detected a negative coherent motion of the clusters. Baffa et al. (1993) reported that galaxies around the Pisces-Perseus supercluster are infalling into the supercluster, i.e., that the supercluster is shrinking. Most recently, Hudson et al. (1997) studied seven clusters in the Pisces-Perseus region and found peculiar motions which are consistent with no bulk motion in the CMB frame. They also argued on the basis of  $\chi^2$ -statistics that their result is also consistent with the negative bulk motion found by Courteau et al. (1993).

We show in Fig.23 mean peculiar velocities derived from our  $H_0$  and  $r_{TF}^c$  corrected for the Malmquist bias. Because of the small number of galaxies at  $V_c < 3000 \text{ km s}^{-1}$ , we discard these galaxies from the current discussion. At a farther region,  $V_c > 8000 \text{ km s}^{-1}$ , we find a serious effect of the sampling incompleteness bias (see Fig.13). The same effect is found in Courteau et al. (1993) and Mathewson and Ford (1994), but they managed to circumvent the effect by comparing the peculiar velocity with that of a control field. As we have no such control data, we simply restrict ourselves to the range of  $3000 \leq V_c \leq 8000 \text{ km s}^{-1}$  for the current discussion on the peculiar motion.

In the  $B$ -band ( $H_0^{(B)} = 65 \text{ km s}^{-1} \text{Mpc}^{-1}$ ) we find a mean negative bulk flow of

$V_p^{(B)} = -744 \pm 92 \text{ km s}^{-1}$ , while a flow with a smaller amplitude  $V_p^{(r)} = -202 \pm 68 \text{ km s}^{-1}$  is obtained in  $r$  ( $H_0^{(r)} = 63 \text{ km s}^{-1} \text{Mpc}^{-1}$ ). If we change  $V_c$  of each galaxies in  $3000 \leq V_c \leq 8000 \text{ km s}^{-1}$  to  $V_c - V_p^{(B)}$  and then re-calculate  $H_0$ , we obtain  $H_0 = 72 \text{ km s}^{-1} \text{Mpc}^{-1}$ . This value is significantly larger than  $H_0^{(B)} = 65 \text{ km s}^{-1} \text{Mpc}^{-1}$ . This naive correction of  $V_c$  for  $V_p^{(B)}$  is probably invalid, however, since it substantially reduces the likelihood. The ratio of the likelihood for  $H_0^{(B)} = 65 \text{ km s}^{-1} \text{Mpc}^{-1}$  to that for  $H_0 = 72 \text{ km s}^{-1} \text{Mpc}^{-1}$  is  $2.6 \times 10^{-6}$ , which indicates less than 0.001% probability for the corrected  $V_c$  being well fitted with the Hubble flow. A 95% probability interval of  $V_p^{(B)}$  inferred from the likelihood ratio is  $-290 \leq V_p^{(B)} \leq +470 \text{ km s}^{-1}$ , each of the boundary corresponding to  $H_0 = 68$  and  $61 \text{ km s}^{-1} \text{Mpc}^{-1}$ , respectively. The inconsistency between the 95% probability interval and  $V_p^{(B)} = -744 \text{ km s}^{-1}$  may be caused by the large uncertainty of the  $B$ -band TF distances due to a large  $\sigma_{TF}^{(B)}$ . It also implies that the current  $B$ -band TF analysis is not suitable for deducing accurate peculiar motions for individual galaxies.

In  $r$ -band, on the other hand, correction of  $V_c$  for  $V_p^{(r)} = -202 \text{ km s}^{-1}$  leads to  $H_0 = 65 \text{ km s}^{-1} \text{Mpc}^{-1}$  which is not significantly different from  $H_0^{(r)} = 63 \text{ km s}^{-1} \text{Mpc}^{-1}$ . Further, a 95% probability interval of  $V_p^{(r)}$  inferred from the likelihood ratio is  $-510 \leq V_p \leq +140 \text{ km s}^{-1}$ , which is consistent with the mean negative bulk flow  $V_p^{(r)} = -202 \text{ km s}^{-1}$ . Boundaries of the 95% probability interval of  $V_p^{(r)}$  corresponds to  $H_0 = 68$  and  $62 \text{ km s}^{-1} \text{Mpc}^{-1}$ , respectively. This consistent result is convincing for the existence of the negative bulk flow. The range of  $V_p$  is consistent with those of the earlier results (Table.5). We consider that the  $r$ -band TF analysis for the peculiar motions seems more reliable than that in  $B$ -band. Our result  $H_0 \sim 65 \text{ km s}^{-1} \text{Mpc}^{-1}$  is also consistent with negative bulk flows which were obtained in the previous studies *independently from an absolute value of  $H_0$* .

## 9. SUMMARY

We perform an unbiased estimate of the global  $H_0$  using a TF relation with a maximum likelihood method. We use a homogeneous, magnitude-limited sample of 441 galaxies ( $m_z \leq 15.5$  mag) distributed up to  $cz \sim 12000 \text{ km s}^{-1}$  in the Pisces-Perseus region. The reliability of the method was examined by the Monte-Carlo simulation, and it was shown that the method works satisfactorily in deriving an unbiased  $H_0$  for the present sample. The results of the present analysis are summarized as follows.

1. We obtain  $H_0^{(B)} = 65 \pm 2^{+20}_{-14} \text{ km s}^{-1} \text{Mpc}^{-1}$  for the unbiased estimate of the global value of the Hubble constant. The first and second error terms represent the internal and external errors, respectively. All the known sources of systematic errors are taken into account in the estimate of the external error. The same analysis with the  $r$ -band TF sample of 271 galaxies gives  $H_0^{(r)} = 63 \pm 1^{+13}_{-7} \text{ km s}^{-1} \text{Mpc}^{-1}$ , which is consistent with  $H_0^{(B)}$ . These  $H_0$ 's are in good agreement with IF92 if we allow for the difference of the TF calibration. We also find a good agreement for these  $H_0$ 's with those obtained via Cepheid observations for local Universe (Freedman 1998), the Tully-Fisher relation (Giovanelli et al. 1997a) and supernovae (Riess, Press and Kirshner 1995, Hamuy et al. 1996) applied to a spatial volume larger than  $\sim 8000 \text{ km s}^{-1}$ .
2. A bulk motion in the Pisces-Perseus region is briefly investigated using our  $H_0$ . Analysis of the  $r$ -band data compiled by Willick et al. (1997) gives a negative motion of  $V_p \sim -200 \text{ km s}^{-1}$  between the range  $3000 \leq V_c \leq 8000 \text{ km s}^{-1}$ . The amplitude of  $V_p$  is consistent with the

95% probability interval  $-510 \leq V_p \leq +140 \text{ km s}^{-1}$  inferred from the likelihood ratio. The interval is consistent with the bulk flows obtained by Willick (1990), Han and Mould (1992), Courteau et al. (1993), and Hudson et al. (1997). Analysis of the *B*-band data does not give a meaningful result because of a larger intrinsic dispersion of the TF relation.

We are grateful to the past and the present staff of the Kiso observatory for taking a number of photographic plates of a good quality. We thank M. Doi, K. Shimasaku, N. Yasuda, N. Kashikawa, and M. Fukugita for their stimulating discussions and valuable suggestions at an early stage of this work. A part of the literature data was taken from Astronomical Data Analysis Center (ADAC) at National Astronomical Observatory of Japan (NAOJ). A part of this work was financially supported in 1994 and 1995 fiscal years by the Research Fellowships of the Japan Society for the Promotion of Science for Young Scientists. We also thank an anonymous referee for many useful suggestions and comments which largely improved an earlier version of this paper.

Criteria	Number of galaxies
Photometry sample	1524
21cm data available	957
Morphological type	754
Inclination	523
Recession velocity	514
21cm line-profile width	<sup>(a)</sup> 449
Absolute magnitude residual	<sup>(b)</sup> 441

Table 1: Sample selection for the Tully-Fisher analysis

Note. — (a) Spiral sample. (b) TF sample.

Name (1)	Type (2)	$\mu$ [mag] (3)	$B_T^0$ [mag] (4)	$r_T^0$ [mag] (5)	$W_{20}^{obs}$ [km s <sup>-1</sup> ] (6)	$V_h$ [km s <sup>-1</sup> ] (7)	$\log R_{25}$ (8)	$M_B - M_{TF}^{(B)}$ [mag] (9)	
									(10)
N224 <sup>†</sup> (M31)	.SAS 3..	<sup>(a)</sup> 24.44 (.13)	3.34 (.02)	2.67	536	-300	0.49	0.13	-0.01
N598 <sup>†</sup> (M33)	.SAS 6..	<sup>(b)</sup> 24.64 (.09)	5.74 (.03)	5.49	199	-179	0.23	0.11	0.09
N300	.SAS 7..	<sup>(c)</sup> 26.66 (.10)	8.53 (.05)	7.89	150	142	0.15	0.48	0.49
N2403	.SXS 6..	<sup>(d)</sup> 27.51 (.24)	8.41 (.07)	7.91	244	131	0.25	0.39	0.34
N3031 <sup>†</sup> (M81)	.SAS 2..	<sup>(e)</sup> 27.80 (.20)	7.40 (.03)	6.36	434	-34	0.28	0.55	0.42
N925	.SXS 7..	<sup>(f)</sup> 29.84 (.16)	10.00 (.11)	—	215	553	0.25	-0.69	-0.72
N3368 (M96)	.SXT2..	<sup>(g)</sup> 30.32 (.16)	9.86 (.13)	—	354	897	0.16	0.38	0.26
N4536	.SXT4..	<sup>(h)</sup> 31.10 (.13)	10.56 (.08)	—	336	1804	0.37	-0.45	-0.53
N1365 <sup>†</sup>	.SBS 3..	<sup>(i)</sup> 31.32 (.17)	9.90 (.07)	8.94	398	1662	0.26	-0.67	-0.79
N4639 <sup>†</sup>	.SXT4..	<sup>(j)</sup> 32.00 (.23)	11.92 (.10)	—	356	1010	0.17	0.72	0.60

Table 2: Local calibrators

Note. — Col(2): Morphological type taken from RC3. Col(3): Distance modulus and its error.  $\mu = 18.50$  mag is assumed for LMC. References are: (a) Freedman and Madore (1990), (b) Freedman, Wilson and Madore (1991), (c) Freedman et al. (1992), (d) Freedman and Madore (1988), (e) Freedman et al. (1994), (f) Silbermann et al. (1996), (g) Tanvir et al. (1995), (h) Saha et al. (1996), (i) Freedman, Madore and Kennicutt (1997), and (j) Sandage et al. (1997). Col(4):  $B$ -band magnitude corrected for the Galactic and the internal extinction and its error taken from RC3. Col(5):  $r$ -band magnitude corrected for the Galactic and the internal extinction prescribed by Willick et al. (1997). Col(6): Observed 21cm line-profile width taken from RC3. Col(7): Heliocentric recession velocity taken from RC3. Col(8): Logarithmic major-to-minor axial ratio taken from RC3. Col(9),(10): Difference between the  $B$ -band absolute magnitude and that derived from the Tully-Fisher relation calibrated with five (col.9) and ten (col.10) calibrators. <sup>†</sup> See text.

	$A_G$		$A_i$		
	RC2–BH	RSA–BH	RC2–RC3	RSA–RC3	Bothun–RC3
TF sample	0.14 (.06)	−0.07 (.07)	−0.12 (.07)	0.36 (.15)	−0.17 (.06)
Local calibrators	0.15 (.05)	−0.06 (.03)	−0.14 (.07)	0.31 (.14)	−0.15 (.03)
Difference	−0.01	−0.01	0.02	0.05	−0.02

Dispersion is given in parentheses.

Table 3: Difference of average extinction corrections for the TF sample

<u>○ Internal random error</u>		
· Statistics (Fig.12)	( $\pm 2 \text{ km s}^{-1} \text{Mpc}^{-1}$ )	$\pm 2.7\%$
<u>○ External systematic error</u>		
· Tully-Fisher calibration	( $\pm 0.20 \text{ mag}$ )	$\pm 9.7\%$
· LMC distance	( $\pm 0.1 \text{ mag}$ )	$\pm 4.6\%$
· Photometric zero point	( $\pm 0.05 \text{ mag}$ )	$\pm 2.3\%$
· Axial ratio	( $\Delta \log R_{25} = 0.03$ )	+9%
· Galactic extinction	( $\pm 0.01 \text{ mag}$ )	$\pm 0.5\%$
· Internal extinction	( $\pm 0.05 \text{ mag}$ )	$\pm 2.3\%$
· Parameters ( $\sigma_{rand}$ , $\Delta W_{20}^{obs}$ , $\Delta \log R_{25}$ , $\Delta B_T$ ) ( $\Delta \log h = 0.005$ )		$\pm 1.2\%$
	(Arithmetic sum)	+30%, −21%

Table 4: Summary of the errors for  $H_0$

	Reference	R.A.	Volume ( $\text{km s}^{-1}$ )	$V_p$ ( $\text{km s}^{-1}$ )
This work	( $B$ , $H_0 = 68 - 61 \text{ km s}^{-1} \text{Mpc}^{-1}$ )	$22^h - 4^h$	3000–8000	(−290, +470)
_____	( $r$ , $H_0 = 63 \text{ km s}^{-1} \text{Mpc}^{-1}$ )	$22^h - 4^h$	3000–8000	$-202 \pm 68$
_____	( $r$ , $H_0 = 68 - 62 \text{ km s}^{-1} \text{Mpc}^{-1}$ )	$22^h - 4^h$	3000–8000	(−510, +140)
Willick (1990)		$22^h - 4^h$	3800–6000	$-441 \pm 49$
Han and Mould (1992)		$0^h - 2^h$	4000–7500	$-420 \pm 115$
Courteau et al. (1993)		$22^h - 4^h$	4000–9000	$-383 \pm 58$
Hudson et al. (1997)		$0^h - 4^h$	4000–6000	$-60 \pm 220$

Table 5: Comparison with previous works of the bulk flow in the Pisces–Perseus region

## REFERENCES

Aaronson, M., Bothun, G., Mould, J., Huchra, J., Schommer, R. A., Cornell, M. E. 1986, *ApJ*, 302, 536

Aaronson, M., Bothun, G., Cornell, M. E., Dawe, J. A., Dickens, R. J., Hall, P. J., Han, M., Huchra, J., Lucey, J. R., Mould, J. R., Murray, J. D., Schommer, R. A., Wright, A. E. 1989, *ApJ*, 338, 654

Baffa, C., Chincarini, G., Henry, R. B. C., Manousyanaki, J. 1993, *A&A*, 280, 20

Bernstein, G. M., Guhathakurta, P., Raychaudhury, S., Giovanelli, R., Haynes, M. P., Herter, T., Vogt, N. P. 1994, *AJ*, 107, 1962

Bothun, G. D., Aaronson, M., Schommer, B., Mould, J. R., Huchra, J., Sullivan III, W. T. 1985, *ApJS*, 57, 423

Bottinelli, L., Gouguenheim, L., Paturel, G., de Vaucouleurs, G. 1983, *A&A*, 118, 4

Bottinelli, L., Fouqué, P., Gouguenheim, L., Paturel, G., Teerikorpi, P. 1987, *A&A*, 181, 1

Bureau, M., Mould, J. R., Staveley-Smith, L. 1996, *ApJ*, 463, 60

Cornell, M. E., Aaronson, M., Bothun, G. D., Mould, J. R. 1987, *ApJS*, 64, 507

Courteau, S., Faber, S. M., Dressler, A., Willick, J. A. 1993, *ApJ*, 412, L51

Davis, M., Peebles, P. J. E. 1983, *ApJ*, 267, 465

de Lapparent, V., Geller, M. J., Huchra, J. P. 1988, *ApJ*, 332, 44

de Vaucouleurs, G., de Vaucouleurs, A., Corwin, H. G., Jr. 1976, Second Reference Catalogue of Bright Galaxies (RC2), (Austin: University of Texas Press)

de Vaucouleurs, G., de Vaucouleurs, A., Corwin, H. G., Jr, Bura, R. J., Paturel, G., Fouqué, P. 1991, Third Reference Catalogue of Bright Galaxies (RC3), (New York: Springer-Verlag)

Faber, S. M., Wegner, G., Burstein, D., Davies, R. L., Dressler, A., Lynden-Bell, D., Terlevich, R. J. 1989, *ApJS*, 69, 763

Fisher, K. B., Davis, M., Strauss, M. A., Yahil, A., Huchra, J. P. 1994, *MNRAS*, 267, 927

Fouqué, P., Bottinelli, L., Gouguenheim, L., Paturel, G. 1990, *ApJ*, 349, 1

Freedman, W. L. 1998, in Proc. IAU symp. 183 on Cosmological Parameters and Evolution of the Universe, in press

Freedman, W. L., Madore, B. F. 1988, *ApJ*, 332, L63

Freedman, W. L., Madore, B. F. 1990, *ApJ*, 365, 186

Freedman, W. L., Madore, B. F., Kennicutt, R. C. 1997, in The Extragalactic Distance Scale (eds. Livio, M., Donahue, M., Panagia, N.), STScI Symp. Ser. 10 (Cambridge: Cambridge University Press)

Freedman, W. L., Wilson, C. D., Madore, B. F. 1991, *ApJ*, 372, 455

Freedman, W. L., Madore, B. F., Hawley, S. L., Horowitz, I. K., Mould, J., Navarrete, M., Sallmen, S. 1992, *ApJ*, 396, 80

Freedman, W. L., Madore, B. F., Mould, J. R., Ferrarese, L., Hill, R., Kennicutt, R. C., Saha, A., Stetson, P., Graham, J. A., Ford, H., Hoessel, J. G., Huchra, J., Hughes, S. M., Illingworth, G. D. 1994, *Nature*, 371, 757

Freudling, W., Da Costa, L. N., Wegner, G., Giovanelli, R., Haynes, M. P., Salzer, J. J. 1995, *AJ*, 110, 920

Freudling, W., Martel, H., Haynes, M. P. 1991, *ApJ*, 377, 349

Fukugita, M., Okamura, S., Tarusawa, K., Rood, H.J., Williams, B. A. 1991, *ApJ*, 376, 8

Fukugita, M., Okamura, S., Yasuda, N. 1993, *ApJ*, 412, L13

Giovanelli, R., Haynes, M. P. 1985, *AJ*, 90, 2445

Giovanelli, R., Haynes, M. P. 1989, *AJ*, 97, 633

Giovanelli, R., Haynes, M. P., Myers, S. T., Roth, J. 1986, *AJ*, 92, 250

Giovanelli, R., Haynes, M. P., Salzer, J. J., Wegner, G., Da Costa, L. N., Freudling, W. 1994, *AJ*, 107, 2036

Giovanelli, R., Haynes, M. P., Da Costa, L. N., Freudling, W., Salzer, J. J., Wegner, G. 1997a, *ApJ*, 477, L1

Giovanelli, R., Haynes, M. P., Herter, T., Vogt, N. P., Wegner, G., Salzer, J. J., Da Costa, L. N., Freudling, W. 1997b, *AJ*, 113, 22

Hamabe, M., Ichikawa, T. 1991, Astronomical Data Analysis Software and Systems I, ASP Conf. Ser., vol.25 (eds. Worrall et al.) (San Franscisco: ASP), 325

Hamuy, M., Phillips, M. M., Maza, J., Suntzeff, N. B., Schommer, R. A., Avilés, R. 1995, *AJ*, 109, 1

Han, M. 1992, *ApJS*, 81, 35

Han, M., Mould, J. R. 1990, *ApJ*, 360, 448

Han, M., Mould, J. R. 1992, *ApJ*, 396, 453

Haynes, M. P., Giovanelli, R. 1986, *ApJ*, 306, L55

Hudson, M. J., Lucey, J. R., Smith, R. J., Steel, J. [astro-ph/9707026](#)

Ichikawa, S., Okamura, S., Watanabe, M., Hamabe, M., Aoki, T., Kodaira, K. 1987, *Ann. Tokyo. Astron. Obs. 2nd Ser.*, 21, 285

Ichikawa, T., Fukugita, M. 1992, *ApJ*, 394, 61 (IF92)

Jacoby, G. H., Branch, D., Ciardullo, R., Davies, R. L., Harris, W. E., Pierce, M. J., Pritchett, C. J., Tonry, J. L., Welch, D. L. 1992, *PASP*, 104, 599

Kirshner, R. P., Kwan, J. 1974, *ApJ*, 193, 27

Kodaira, K., Okamura, S., Ichikawa, S., Hamabe, M., Watanabe, M. 1990, Photometric Atlas of Northern Bright Galaxies, (Tokyo: University of Tokyo Press)

Kolatt, T., Dekel, A., Ganon, G., Willlick, J. A. 1996, ApJ, 458, 419

Landolt, A. U. 1992, AJ, 104, 340

Lauberts, A., Valentijn, E. A. 1989, The Surface Photometry Catalogue of the ESO-Uppsala Galaxies, (Munich: European Southern Observatory)

Livio, M., Donahue, M., Panagia, N., eds 1997, The Extragalactic Distance Scale, STScI Symp. Ser. 10 (Cambridge: Cambridge University Press)

Longo, G., de Vaucouleurs, A. 1983, A General Catalogue of Photoelectric Magnitudes and Colors in the U,B,V System of 3,578 Galaxies Brighter Than the 16-th V-magnitude (1936-1982), (Austin: University of Texas)

Loveday, J., Peterson, B. A., Efstathiou, G., Maddox, S. J. 1992, ApJ, 390, 338

Madore, B. F., Freedman, W. L. 1991, PASP, 103, 933

Malmquist, K. G. 1922, Med.Lunds.Astr.Obs, 16, No.23

Marzke, R. O., Huchra, J. P., Geller, M. J. 1994, ApJ, 428, 43

Mathewson, D. S., Ford, V. L. 1994, ApJ, 434, L39

McMillan, R., Ciardullo, R., Jacoby, G. H. 1993, ApJ, 416, 62

Nilson, P. 1973, Uppsala General Catalogue of Galaxies (UGC), (Uppsala: Uppsala Obs. Ann.)

Okamura, S. 1998, in Proc. The 11th Nishinomiya-Yukawa Memorial Symposium on 'Physics in the 21st Century'

Pierce, M. J. 1991, in Observational Tests of Cosmological Inflation (eds. Shanks, T., Banday, A., Ellis, R. S., Frenk, C. S., Wolfendale, A. W.) (Dordrecht: Kluwer)

Pierce, M. J. 1994, ApJ, 430, 53

Pierce, M. J., Tully, R. B. 1988, ApJ, 330, 579

Pierce, M. J., Tully, R. B. 1992, ApJ, 387, 47

Pierce, M. J., Welch, D. L., McClure, R. D., van den Bergh, S., Racine, R., Stetson, P. B. 1994, Nature, 371, 385

Riess, A. G., Press, W. H., Kirshner, R. P. 1995, ApJ, 438, L17

Saha, A., Sandage, A., Labhardt, L., Schwengeler, H., Tammann, G. A., Panagia, N., Macchetto, F. D. 1995, ApJ, 438, 8

Saha, A., Sandage, A., Labhardt, L., Tammann, G. A., Macchetto, F. D., Panagia, N. 1996, ApJ, 466, 55

Sandage, A., Tammann, G. A. 1981, A Revised Shapley-Ames Catalog of Bright Galaxies (RSA), (Washington: Carnegie Inst. of Washington Pub.)

Sandage, A. et al. 1997, ApJ submitted.

Schechter, P.L., 1980, AJ, 85, 801

Schmidt, B. P., Kirshner, R. P., Eastman, R. G., Phillips, M. M., Suntzeff, N. B., Hamuy, M., Maza, J., Avilés, R. 1994, ApJ, 432, 42

Shanks, T. 1997, MNRAS, 290, L77

Silbermann, N. A., Harding, P., Madore, B. F., Kennicutt, R. C., Saha, A., Stetson, P. B., Freedman, W. L., Mould, J. R., Graham, J. A., Hill, R. J., Turner, A., Bresolin, F., Ferrarese, L., Ford, H., Hoessel, J. G., Han, M., Huchra, J., Hughes, S. M., Illingworth, G. D., Phelps, R., Sakai, S. 1996, ApJ, 470, 1

Smoot, G. F., Bennett, C. L., Kogut, A., Aymon, J., Backus, C., de Amici, G., Galuk, K., Jackson, P. D., Keegstra, P., Rokke, L., Tenorio, L., Torres, S., Gulkis, S., Hauser, M. G., Janssen, M. A., Mather, J. C., Weiss, R., Wilkinson, D. T., Wright, E. L., Boggess, N. W., Cheng, E. S., Kelsall, T., Lubin, P., Meyer, S., Moseley, S. H., Murdock, T. L., Shafer, R. A., Silverberg, R. F. 1991, ApJ, 371, L1

Strauss, M. A., Willick, J. A. 1995, Phys. Rep., 261, 271

Tammann, G. A., Sandage, A. 1995, ApJ, 452, 16

Tanvir, N. R., Shanks, T., Ferguson, H. C., Robinson, D. R. T. 1995, Nature, 377, 27

Tonry, J. L., Blakeslee, J. P., Ajhar, E. A., Dressler, A. 1997, ApJ, 475, 399

Tully, R. B., Fisher, J. R. 1977, A&A, 54, 661

van den Bergh, S. 1994, PASP, 106, 1113

Watanabe, M. 1996, Ph.D. thesis, University of Tokyo

Willick, J. A. 1990, ApJ, 351, L5

Willick, J. A. 1991, Ph.D. thesis, University of California

Willick, J. A., Courteau, S., Faber, S. M., Burstein, D., Dekel, A., Strauss, M. A. 1997, ApJS, 109, 333

Yasuda, N., Okamura, S., Fukugita, M. 1995, ApJS, 96, 359

Zwicky, F., Herzog, E., Wild, P., Karpowicz, M., Kowal, C. T. 1961-68, Catalogue of Galaxies and of Clusters of Galaxies (CGCG), (Pasadena: California Institute of Technology)

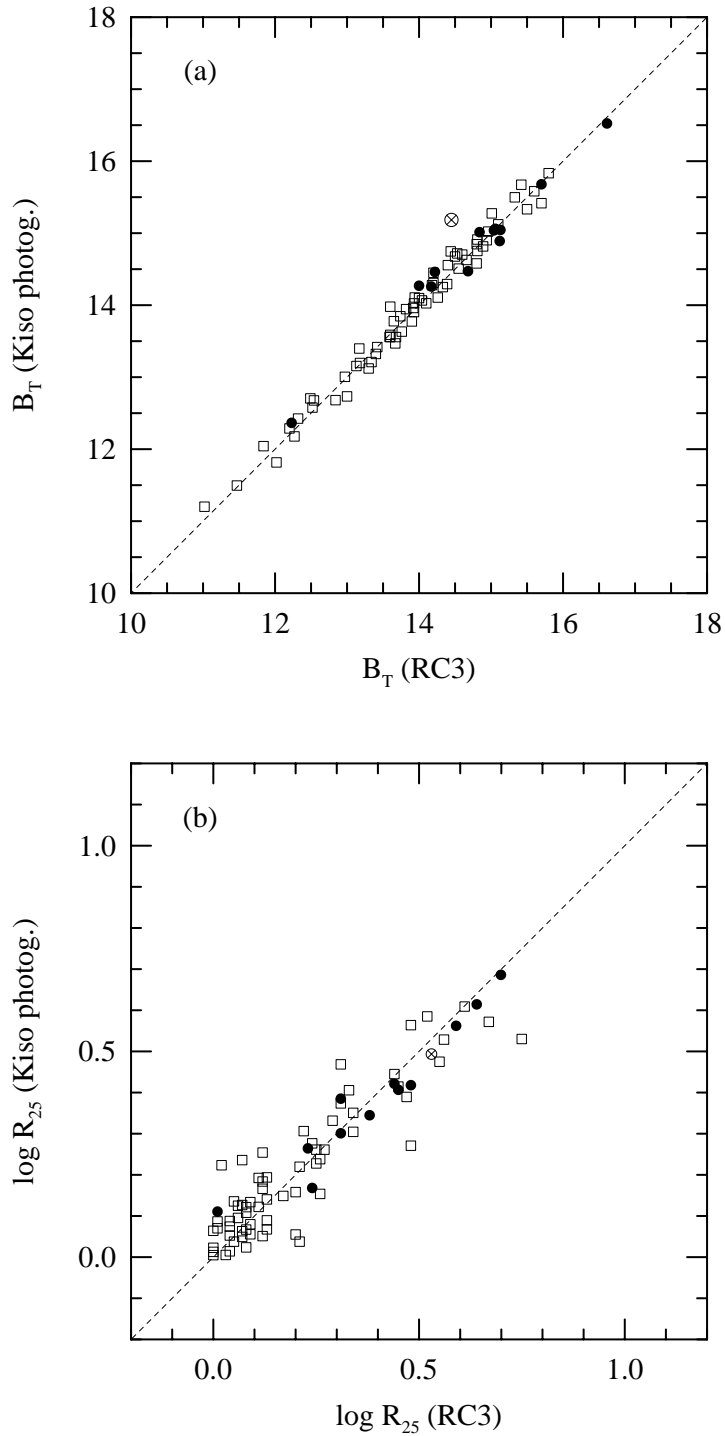
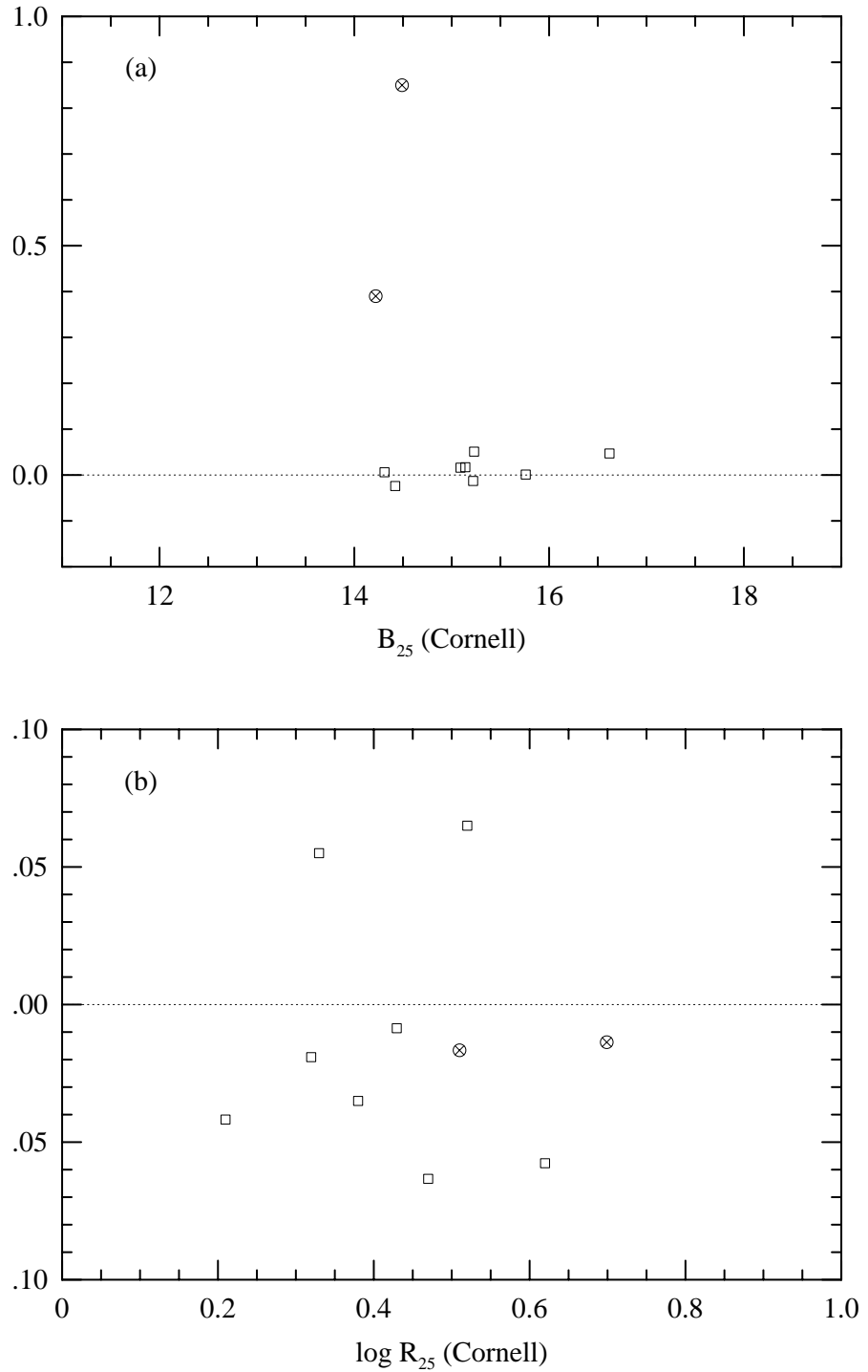


Fig. 1.— Comparisons (a) of the total magnitude  $B_T$  and (b) of the logarithmic isophotal major-to-minor axial ratio  $\log R_{25}$ , between RC3 data and ours. Filled circles represent galaxies for which RC3 data are based on surface photometry. A encircled cross indicates PGC 5473 (see text).



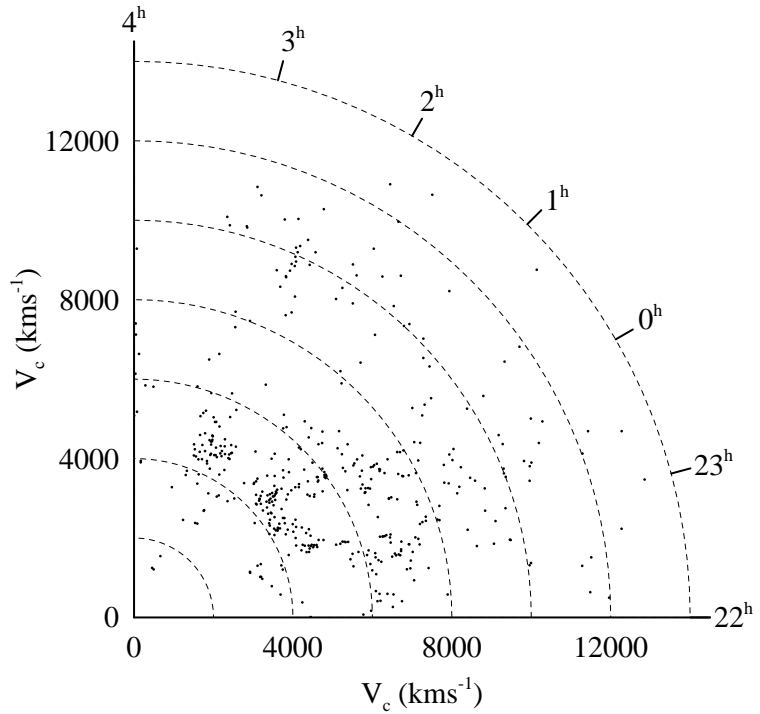


Fig. 3.— Velocity distribution of the spiral sample ( $N = 449$ ). The velocity is expressed in the CMB-rest frame.

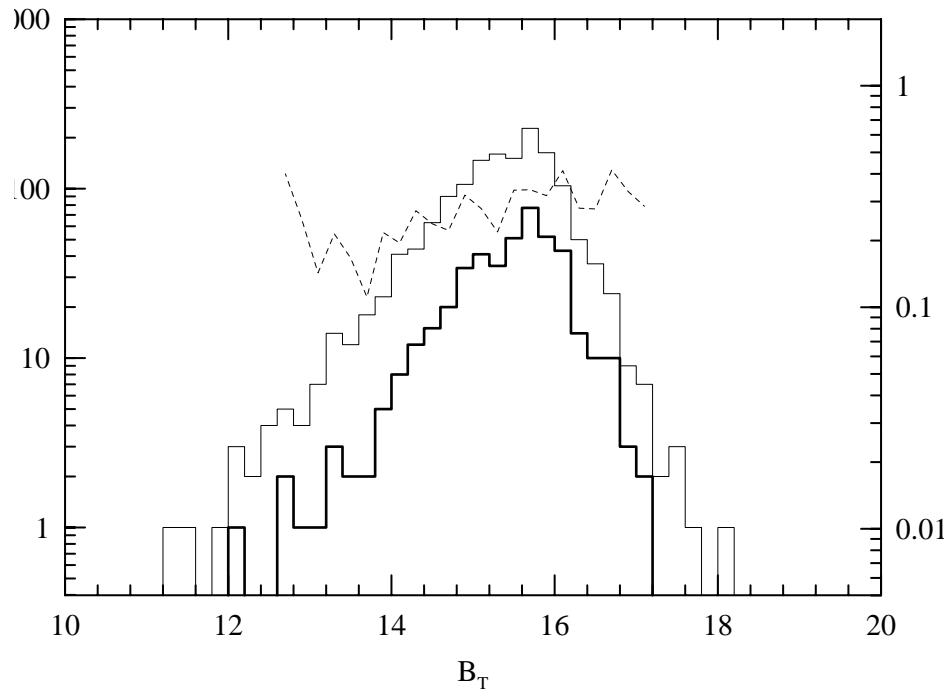


Fig. 4.— A histogram of the total magnitude  $B_T$  for the spiral sample ( $N = 449$ , thick line) and the photometry sample ( $N = 1524$ , thin line). A dashed line shows a number ratio of the former sample to the latter.

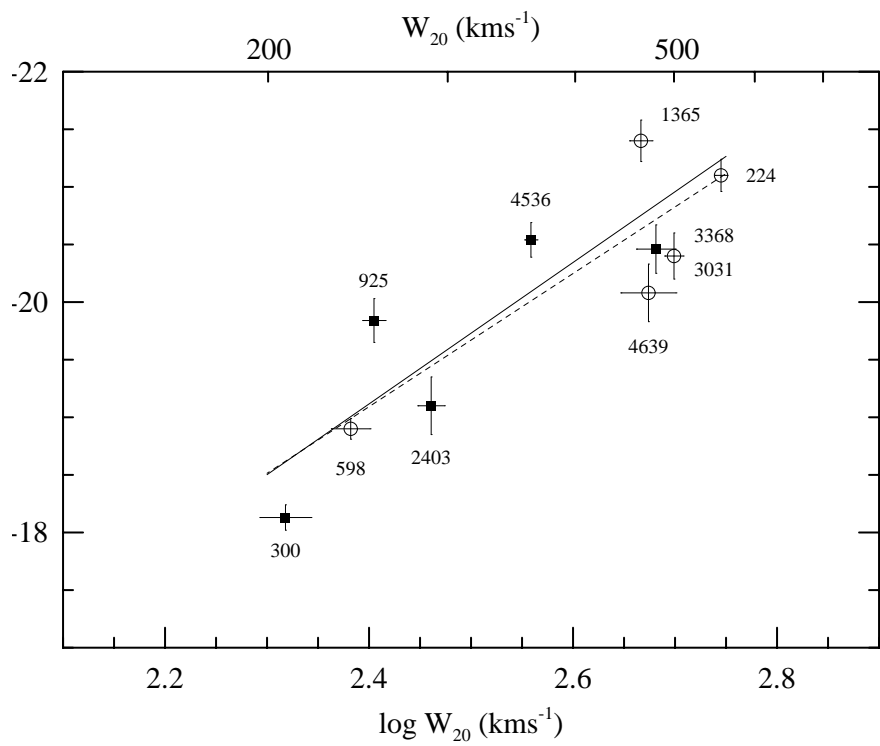


Fig. 5.— The  $B$ -band Tully-Fisher diagram for the local calibrators given in Table 2. The NGC number is labeled. Open circles represent five galaxies discarded from the fiducial calibration (see text). The solid and dashed lines show regression lines for the fiducial set of five calibrators and for all the ten calibrators, respectively.

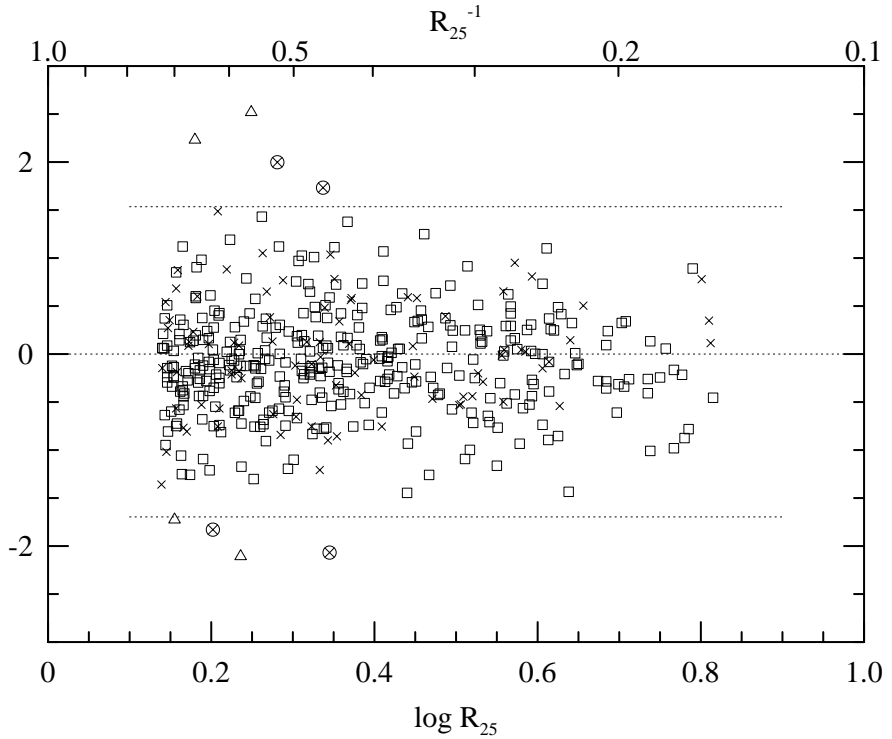


Fig. 6.— Difference between the TF magnitude  $M_{TF}^{(B)}$  and the magnitude  $M_B$  from the Hubble's law with  $\log h = -0.15$ , plotted against  $\log R_{25}$  for the spiral sample ( $N = 449$ ). Crosses represent galaxies whose images are contaminated by other images. Upper and lower dashed lines delineate the boundaries  $|M_{TF}^{(B)} - M_B| = 1.62$  mag. Eight galaxies (encircled crosses and triangles) are out of the boundaries and hence discarded from the TF analysis. The enclosed crosses indicate galaxies with unreliable observational data (see text).

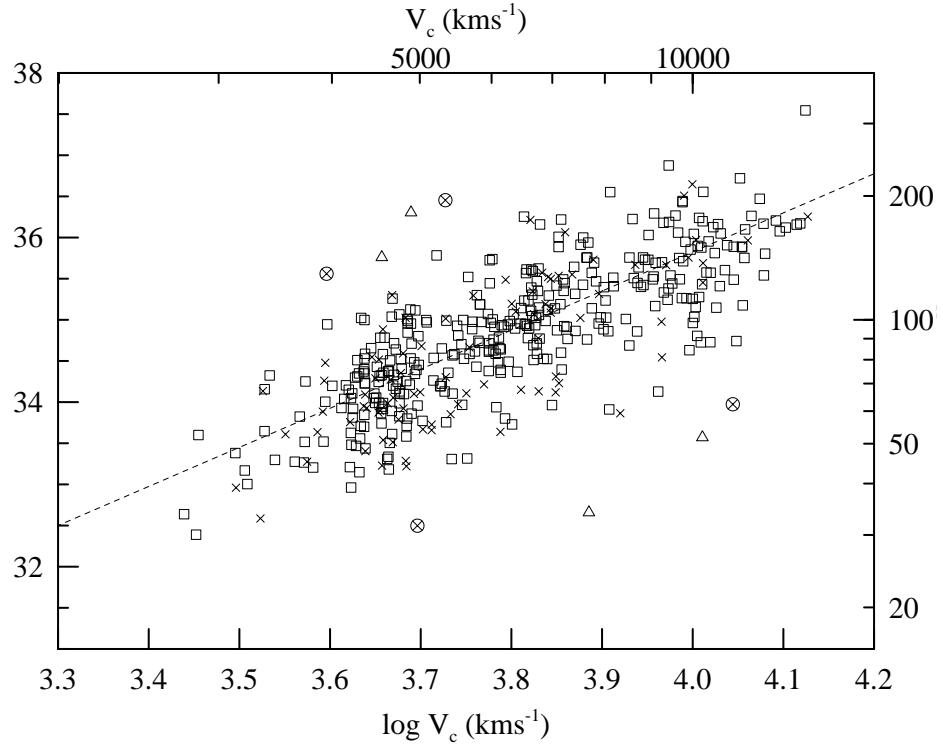


Fig. 7.— The velocity-TF distance relation for the spiral sample ( $N = 449$ ). Symbols are the same as in Fig.6. A dashed line represents an arbitrary Hubble's law with  $\log h = -0.15$ .

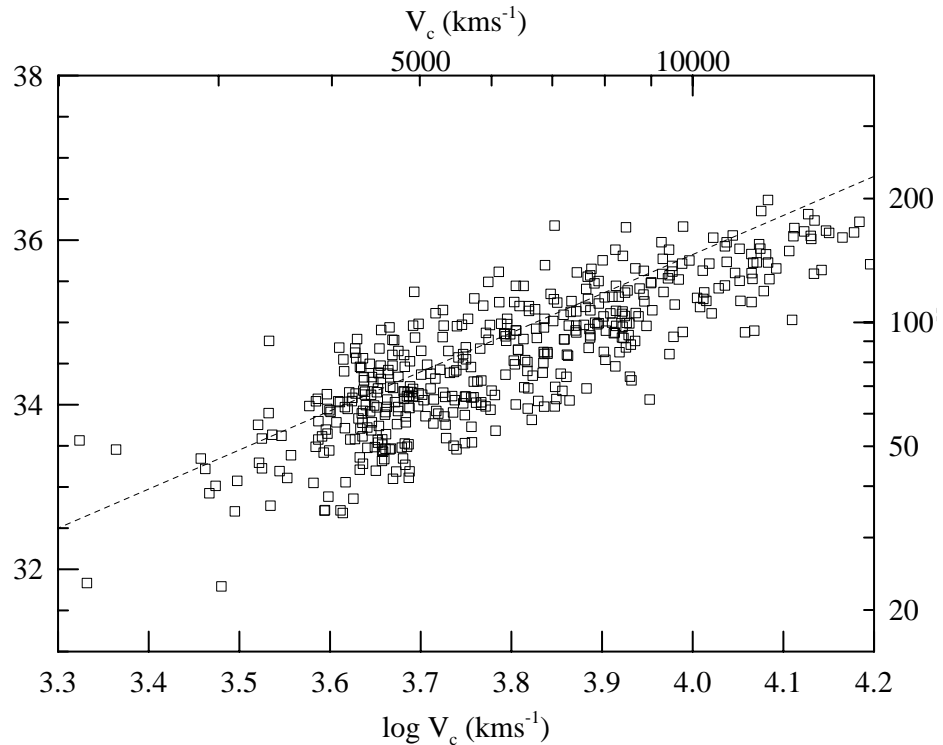


Fig. 8.— Same as Fig.7 but for one of the simulated TF samples ( $N = 441$ ).

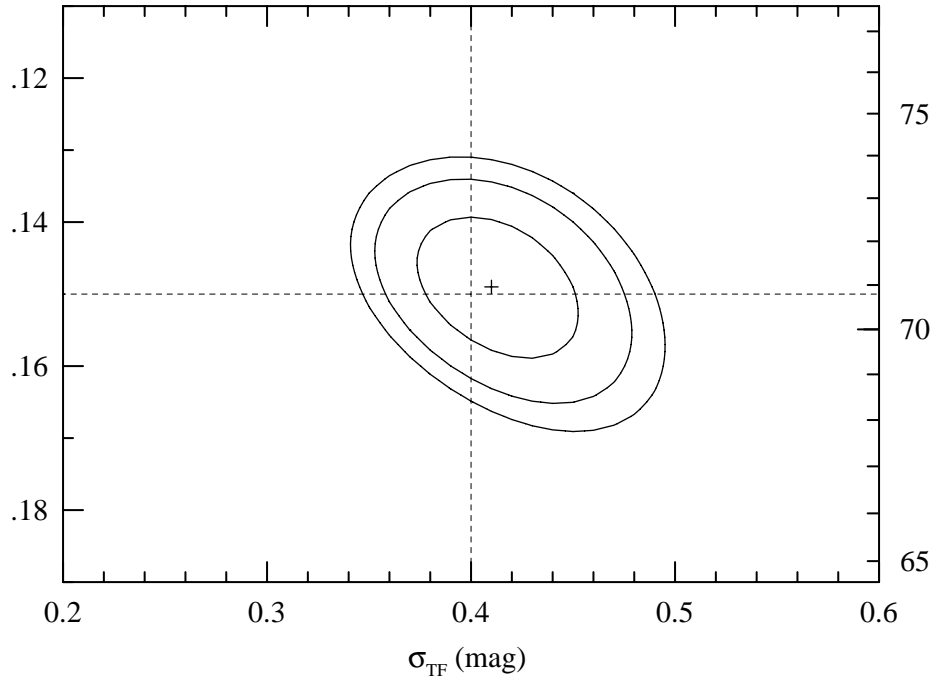


Fig. 9.— Probability contour map for  $H_0$  and  $\sigma_{TF}$  obtained from one of the simulated TF samples. Confidence levels at 70%, 95% and 99% are shown. Horizontal and vertical dashed lines indicate the input values  $\log h = -0.15$  and  $\sigma_{TF} = 0.40$  mag, respectively, which are assumed a priori for the simulated sample.

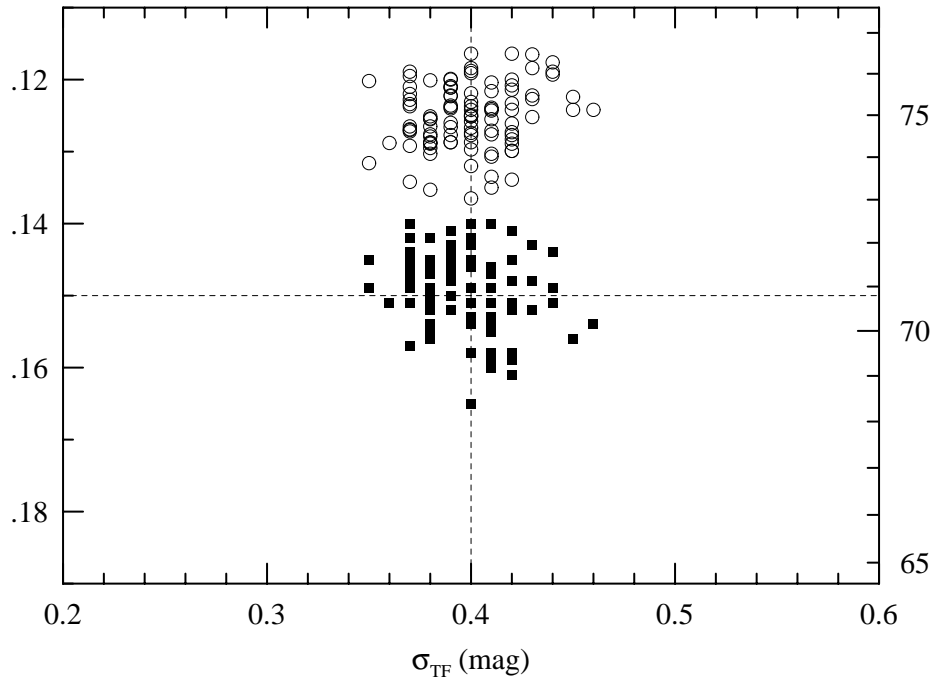


Fig. 10.— The most probable values of  $H_0$  and  $\sigma_{TF}$  for one hundred different simulated TF samples. Filled squares represent those obtained by the maximum likelihood method, while open circles represent sample averages of  $\log(V_c/r_{TF})$  for  $\log h$  with  $\sigma_{TF}$  a priori set equal to that obtained with the maximum likelihood method.

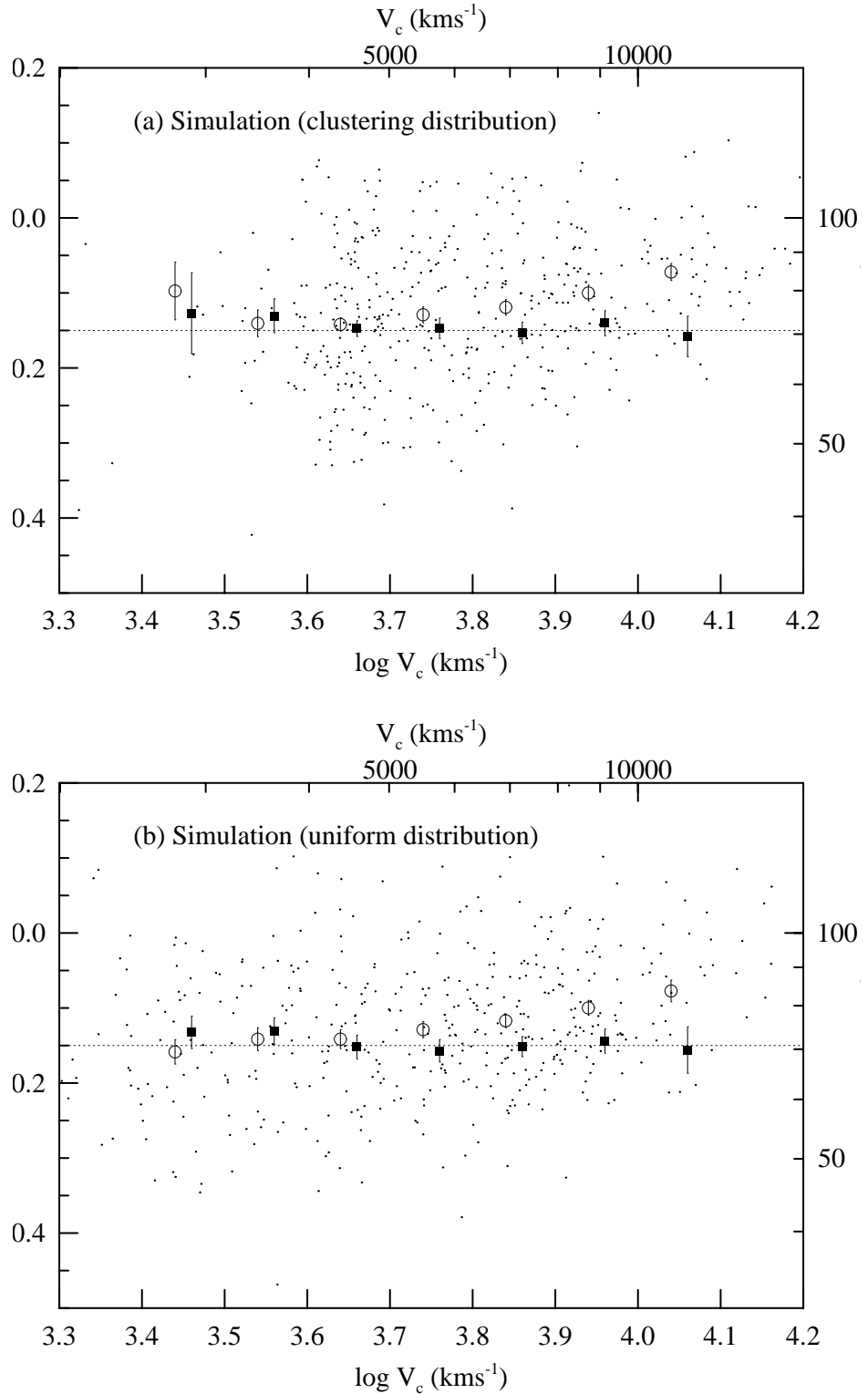


Fig. 11.— Spatial variation of  $H_0$  obtained (a) from the simulated TF sample shown in Fig.9 and (b) from a simulated TF sample with an uniform spatial distribution. The intrinsic scatter  $\sigma_{TF}$  is fixed at 0.41 mag for all the subsamples in  $\log V_c$  bins. Dots represent the individual galaxies, to which the Hubble ratio  $V_c/r_{TF}$  is given as  $H_0$ . Filled squares represent the most probable  $H_0$  in each bin obtained by the maximum likelihood method, while open circles represent the sample average of  $\log(V_c/r_{TF})$ . The squares and the circles are shifted from the center of each  $\log V_c$  bin to avoid the overlap. Error bars are taken from the 70% error obtained for each subsample. A dashed line indicates the input value  $\log h = -0.15$ .

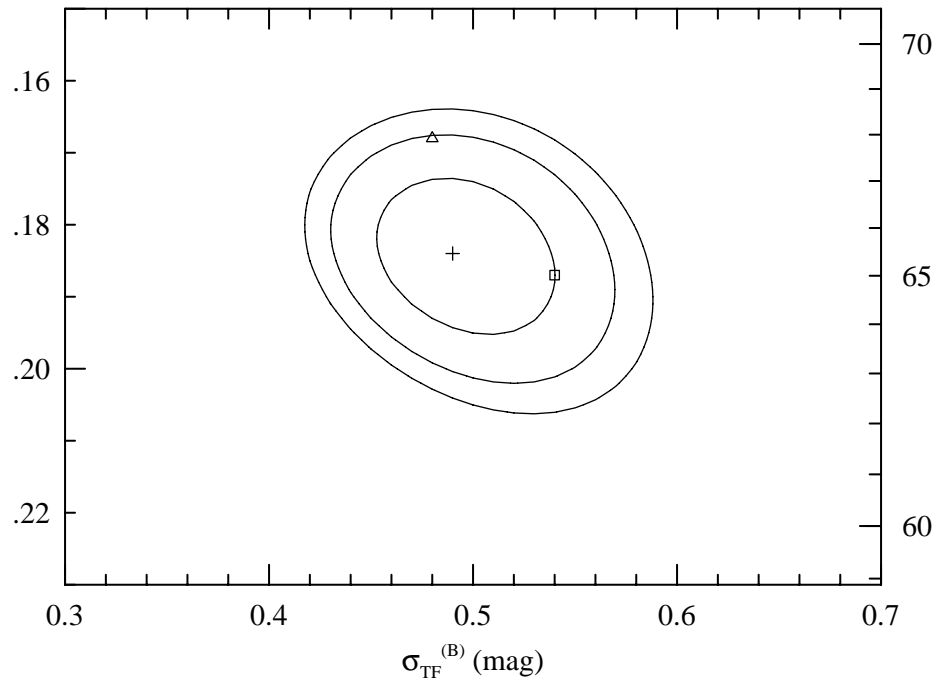


Fig. 12.— Probability contour map for  $H_0$  and  $\sigma_{TF}^{(B)}$  for the TF sample of 441 galaxies. A plus indicates the most probable values. Contours are drawn at 70%, 95% and 99% confidence levels. A triangle and a square indicate the results obtained from the ten calibrators and from the inclusion of four deviant galaxies, respectively (see text).

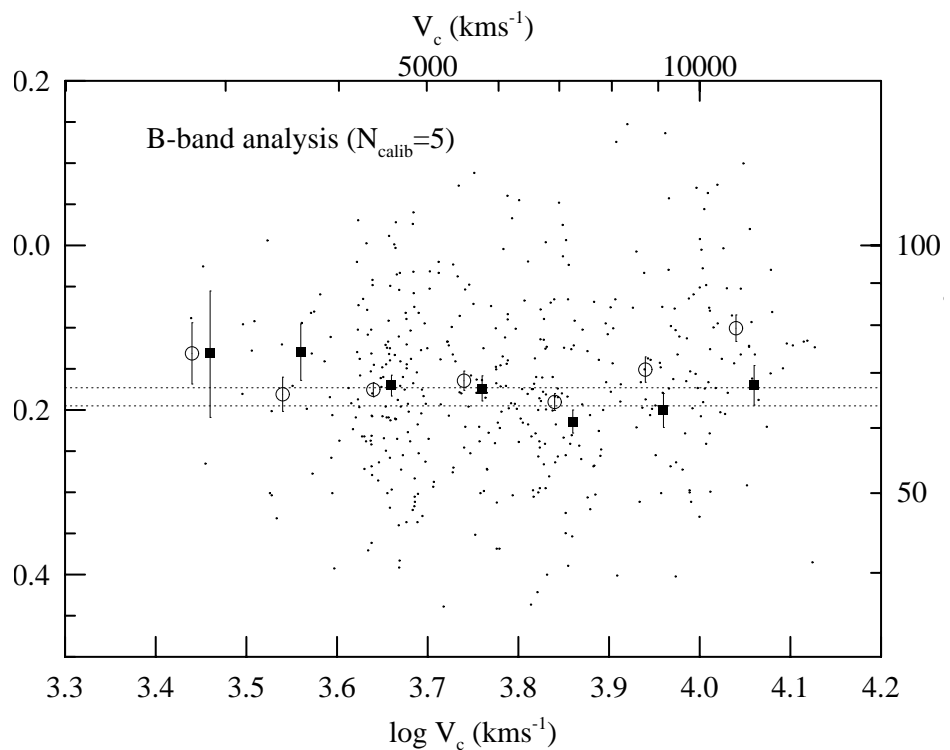


Fig. 13.— Spatial variation of  $H_0$  obtained from the TF sample. The intrinsic scatter  $\sigma_{TF}^{(B)}$  is fixed at 0.49 mag for all the subsamples in  $\log V_c$  bins. Dots represent the individual galaxies, to which the Hubble ratio  $V_c/r_{TF}^{(B)}$  is given as  $H_0$ . Filled squares represent the most probable  $H_0$  in each bin obtained by the maximum likelihood method, while open circles represent the sample average of  $\log(V_c/r_{TF}^{(B)})$ . The squares and the circles are shifted from the center of each  $\log V_c$  bin to avoid the overlap. Error bars are taken from the 70% error obtained for each subsample. Two dashed lines indicate the 70% confidence levels  $H_0 = 63$  and  $67 \text{ km s}^{-1} \text{Mpc}^{-1}$  shown in Fig. 12.

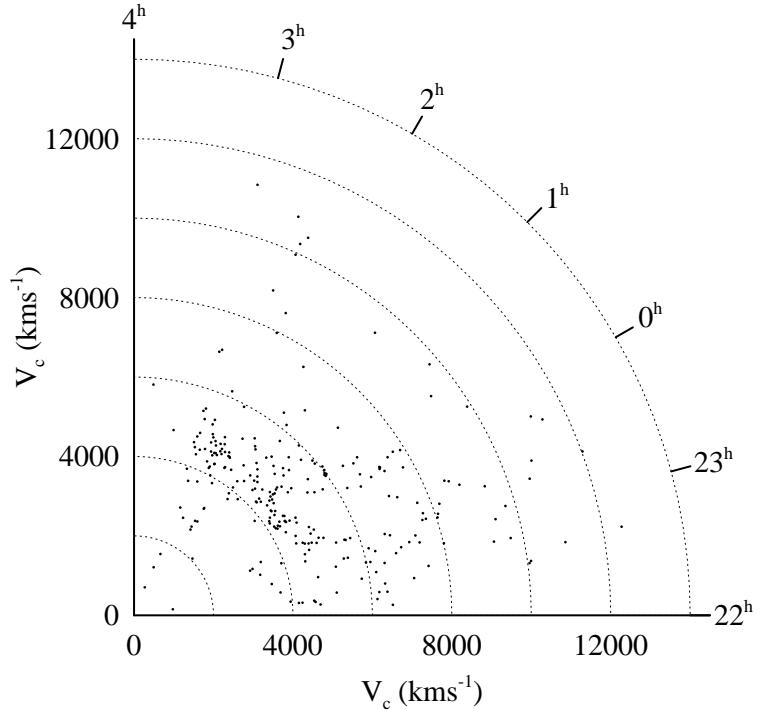


Fig. 14.— Velocity distribution of the  $r$ -band TF sample ( $N = 271$ ). The velocity is expressed in the CMB-rest frame.

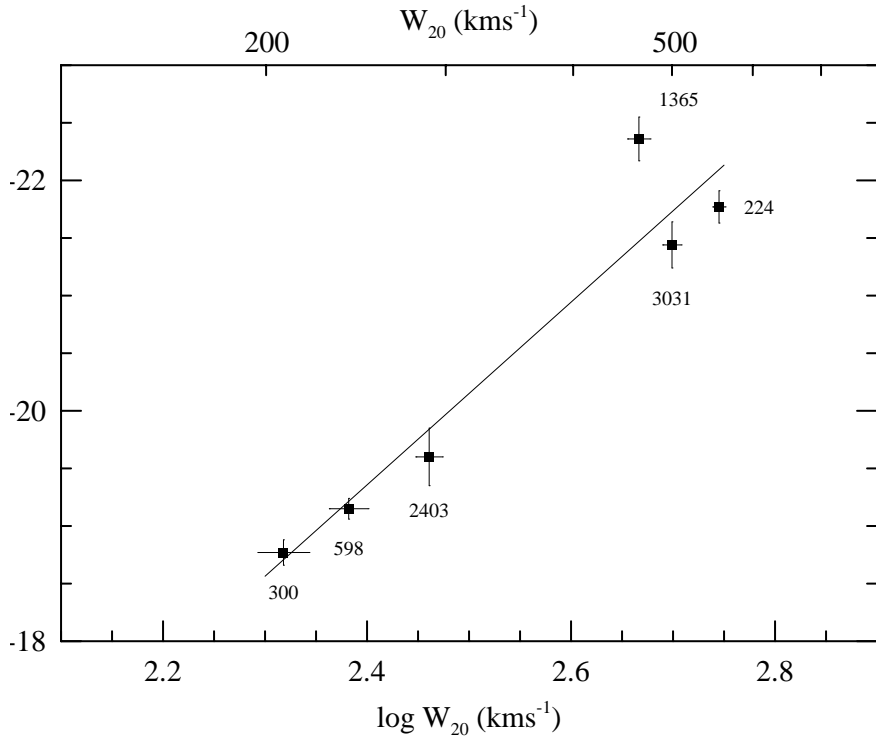


Fig. 15.— The  $r$ -band Tully-Fisher diagram for the local calibrators given in Table 2. The NGC number is labeled. The regression line shows equation (18).

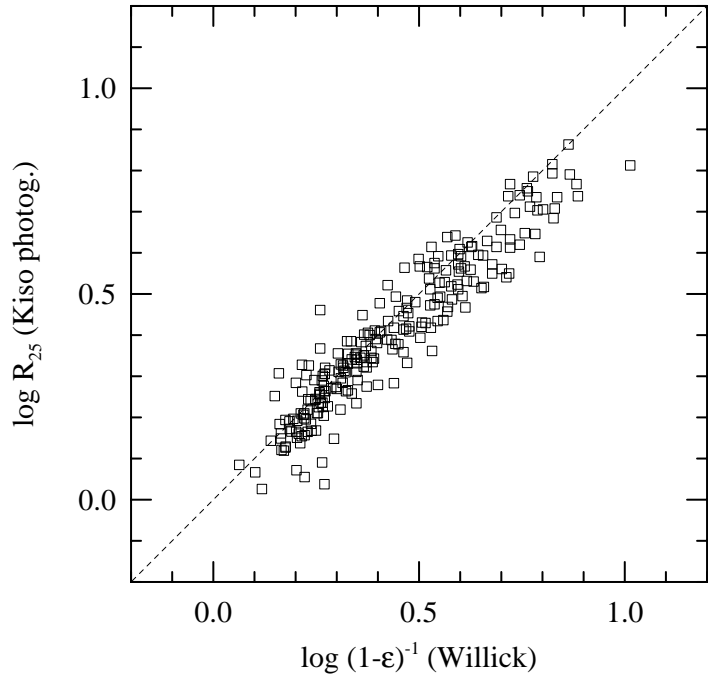


Fig. 16.— A comparison of the major-to-minor axial ratios between the data of Willick (1991) and ours.

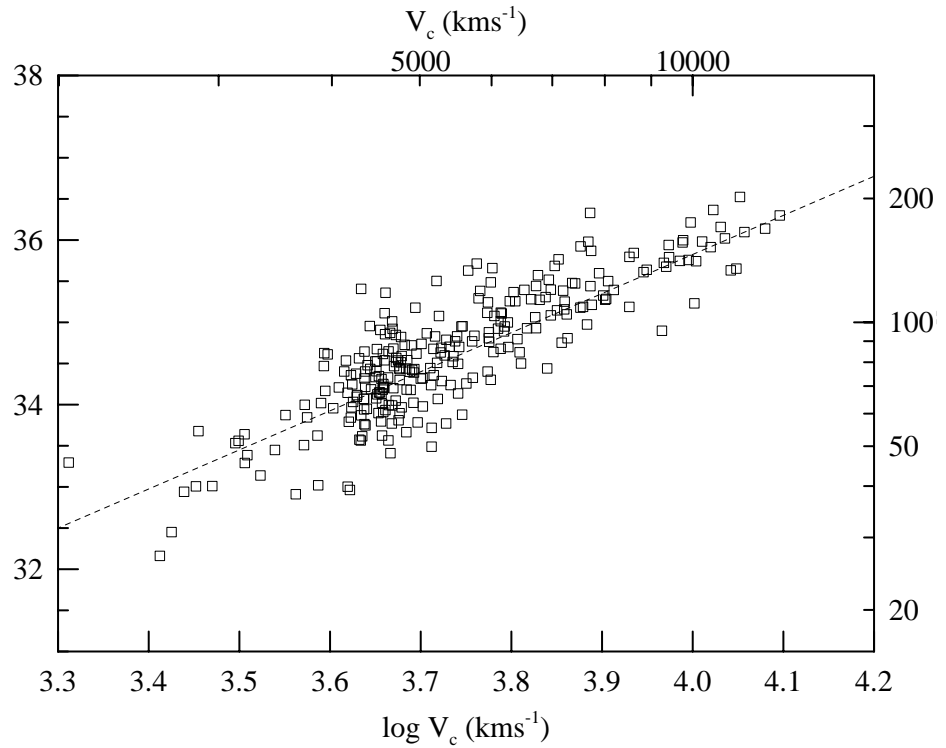


Fig. 17.— The velocity-TF distance relation for the  $r$ -band TF sample. A dashed line represents an arbitrary Hubble's law with  $\log h = -0.15$ .

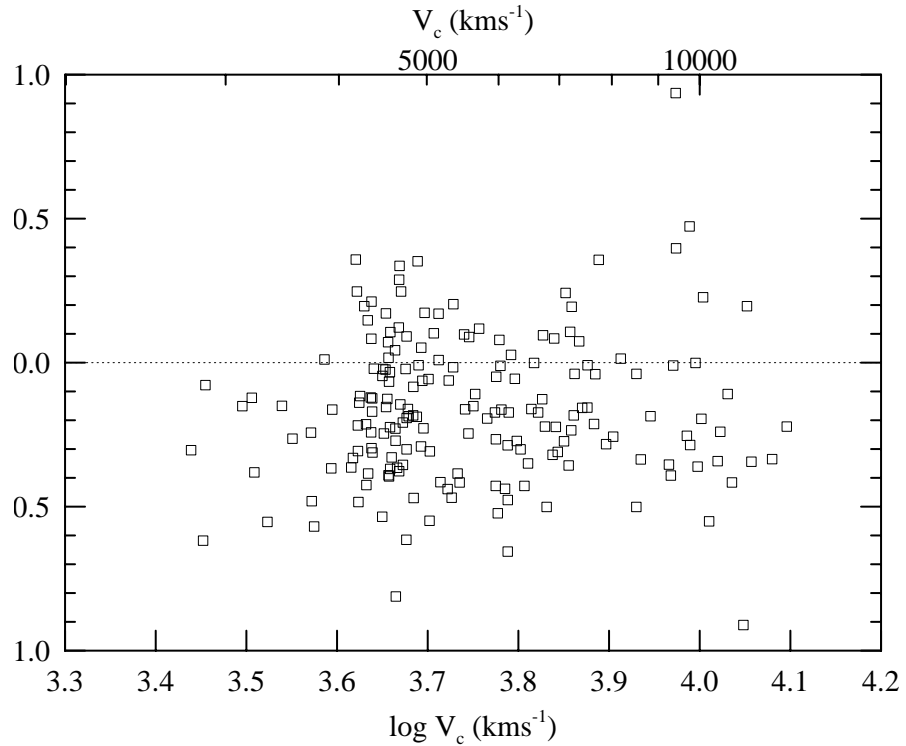


Fig. 18.— Difference between the TF distance moduli  $\mu_{TF}^{(B)}$  and  $\mu_{TF}^{(r)}$ .

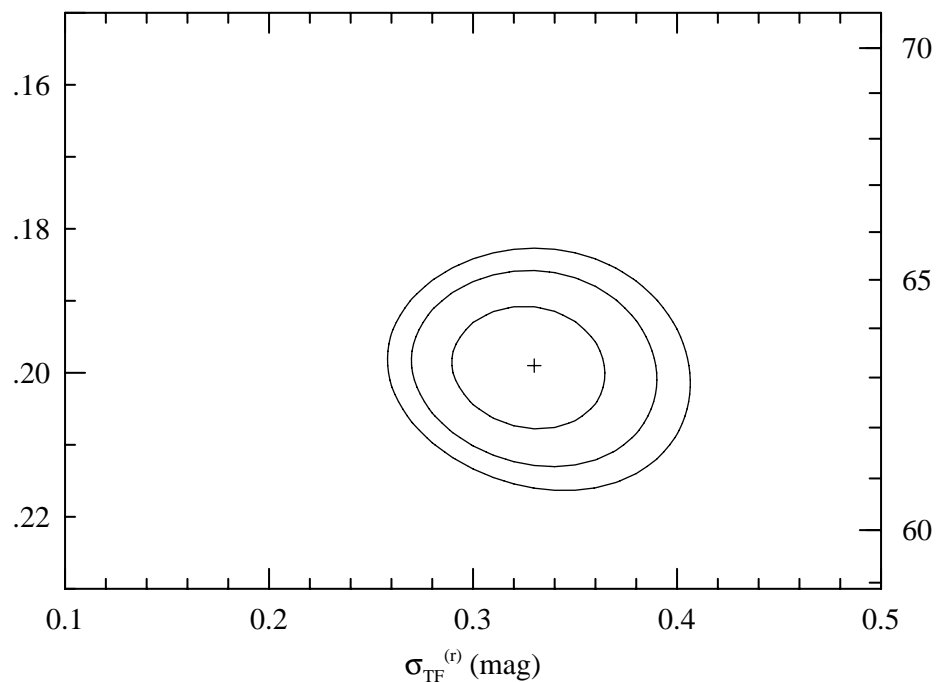


Fig. 19.— A probability contour map for  $H_0$  and  $\sigma_{TF}^{(r)}$  obtained from the  $r$ -band TF sample. Confidence levels at 70%, 95% and 99% are shown.

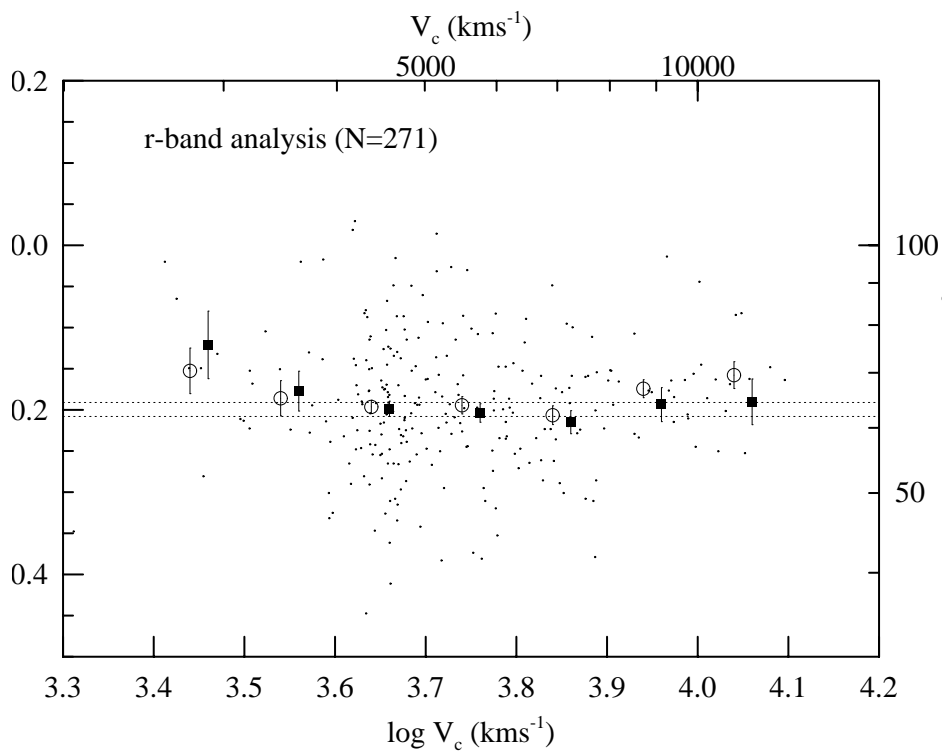


Fig. 20.— Spatial variation of  $H_0$  obtained from the  $r$ -band TF sample. The intrinsic scatter  $\sigma_{TF}^{(r)}$  is fixed for all the subsamples in  $\log V_c$  bins to 0.33 mag obtained in Fig.19. Dots represent the individual galaxies, to which the Hubble ratio  $V_c/r_{TF}^{(r)}$  is given as  $H_0$ . Filled squares represent the most probable  $H_0$  in each bin obtained by the maximum likelihood method, while open circles represent the sample average of  $\log(V_c/r_{TF}^{(r)})$ . The squares and the circles are shifted from the center of each  $\log V_c$  bin to avoid the overlap. Error bars are taken from the 70% error obtained for each subsample. Two dashed lines indicate the 70% confidence levels  $H_0 = 62$  and  $64 \text{ km s}^{-1} \text{Mpc}^{-1}$  shown in Fig.19.

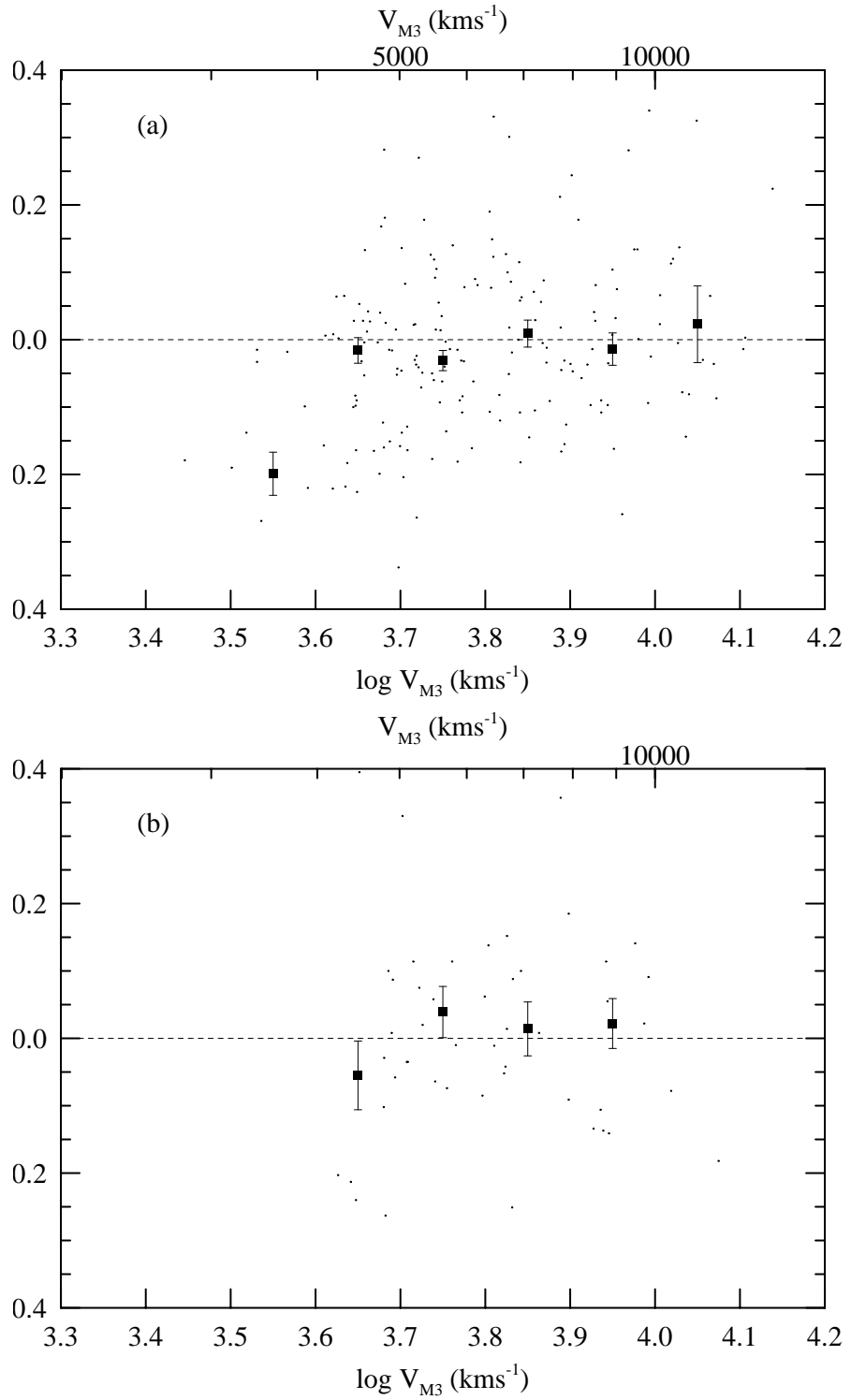


Fig. 21.— Relative difference of the Hubble velocity between Mark III catalog (Willick et al. 1997) and ours, plotted against the Mark III Hubble velocity. (a) “w91pp” (b) “hmcl”. Dots represent individual galaxies and solid squares show median in each  $\log V_{M3}$  bin. Error bars are calculated as a standard deviation divided by a square root of the number of galaxies in each bin.

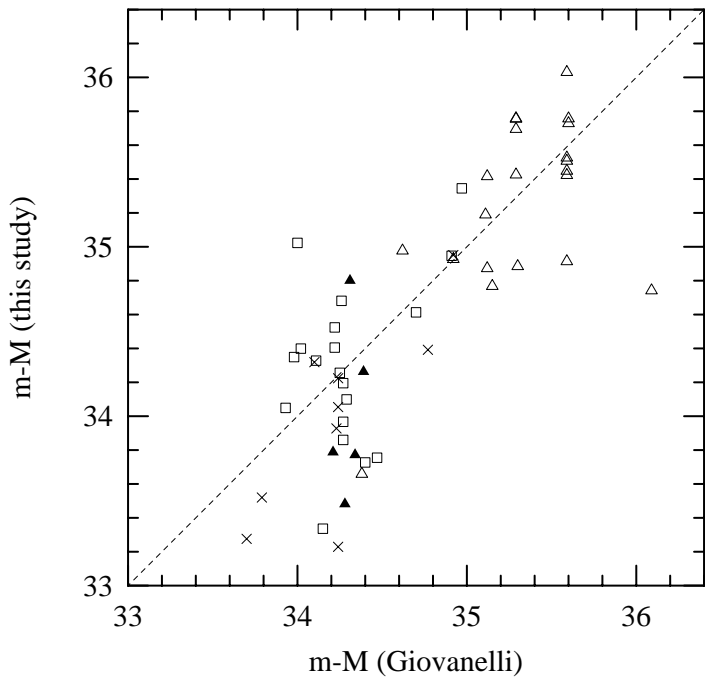


Fig. 22.— Comparison of the distance modulus between Giovanelli et al. (1997b) and this study. Squares, crosses, closed and open triangles represent galaxies in NGC 383 group, NGC 507 group, A 262, and A 2634/A 2666, respectively. Distance moduli for their galaxies are based on  $H_0 = 69 \text{ km s}^{-1} \text{Mpc}^{-1}$  from Giovanelli et al. (1997a).

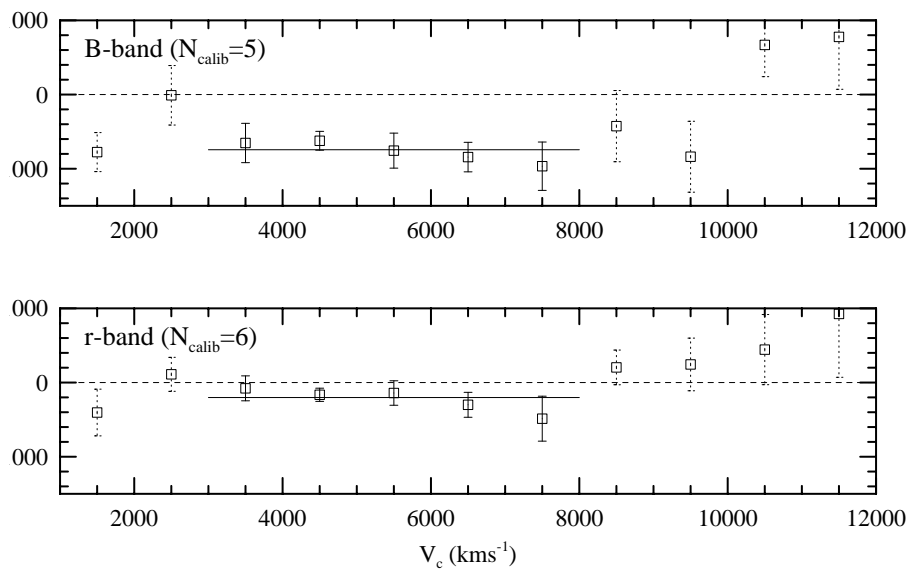


Fig. 23.— Peculiar velocities plotted against the CMB-rest recession velocity in  $B$  (upper) and  $r$  (lower). A solid horizontal line shows a mean value ( $V_p^{(B)} = 744 \text{ km s}^{-1}$  in  $B$  and  $V_p^{(r)} = 202 \text{ km s}^{-1}$  in  $r$ ) in the range  $3000 \leq V_c \leq 8000 \text{ km s}^{-1}$ .